Chapter 2

# Applications of Switch-Mode Rectifiers on Micro-grid Incorporating with EV and BESS

K. W. Hu and C. M. Liaw

Additional information is available at the end of the chapter

http://dx.doi.org/10.5772/61248

**Abstract**

A switch-mode rectifier (SMR) can provide adjustable and well-regulated DC output voltage from the available AC source with good line drawn power quality. Depending on the input/output voltage transfer characteristics, the schematics, the operation quadrant, and control, SMRs possess many classifications and application. Typical potential application examples include grid powered motor drives, battery chargers, various power electronic facilities, micro-grids, and grid-connected battery energy storage system (BESS), etc. In micro-grids, the SMR can be employed as the AC generator-followed converter to yield better generating efficiency. The SMR operation of its grid-connected inverter let the grid-to-microgrid (G2M) operation be conductable in addition to the microgrid-to-grid (M2G) operation. As for the electric vehicle (EV), the bidirectional inverter can be arranged to perform G2V/V2G operations in idle case, wherein the SMR operation is made in G2V battery charging.

To promote the application potential and improve the operation performance of SMRs, this article presents the operation controls and applications of SMRs in micro-grid systems incorporating BESS and EV as supplemental facilities. First, the classifications, operation principle, and some key issues of SMRs are explored. Secondly, the configuration of the studied system is introduced. Third, the controls and operations of SMRs in micro-grid, wind generators, and grid-connected interface power converters are described. Then the ones in BESS (B2G/G2B) and EV are introduced. Finally, some conclusions and suggestions are given.

**Keywords:** Power quality, power factor correction, switch-mode rectifier, control, micro-grid, BESS, electric vehicle, battery charger

## 1. Introduction

Energy exhaustion, carbon-dioxide emission, and global warming issues have seriously received attention worldwide in recent years. The use of micro-grid [1-4] incorporating with various distributed and renewable sources and energy storage devices is an effective means to reduce these problems. Compared with the AC micro-grid, the DC micro-grid possesses the merits of simpler interface converters, allowing longer common DC bus length and having fewer losses [1]. For establishing a high-performance micro-grid, many interdisciplinary affairs should be properly treated, such as:

**i.** Interfacing the renewable sources to the system with proper interface converters and controls. Each specific source possesses its own key issues to be adequately handled. For a wind AC generator, the SMR is a natural choice to yield better energy conversion characteristics;

**ii.** Equipped with proper storage devices and their coordinated controls. If the auxiliary charging from the mains is arranged, the SMR must also be adopted to have good charging performance and line drawn power quality; and

**iii.** Energy management control for the constituted sources, storage devices, and loads. Recently, many droop control approaches [1,5] have been developed to enhance the autonomous operation control characteristics of micro-grids.

Similar to micro-grids, the popularization of electric vehicles (EVs) [6] is also effective in reducing fossil energy consumption and carbon-dioxide emission. Moreover, by regarding EV as a movable energy storage device and performing its interconnected operations to a micro-grid (M2V/V2M) [7,8] or utility grid (G2V/V2G) [9-14], the effectiveness in achieving these goals will be more prominent. Among the commonly used motors, permanent-magnet synchronous motor (PMSM) is one of the commonly used motors for commercialized EVs [15,16], owing to its many distinguished features. Battery is the major source of an EV, hence its type and ratings should be properly chosen [17-19]. Different from the energy type of battery, the super-capacitor belongs to the power type energy storage device that has faster response and lower capacity. By incorporating battery with super-capacitor, one can preserve better total energy utilization characteristics. Then, intermittent battery charging/discharging operations can be avoided to increase battery life. The super-capacitor can be directly paralleled to the battery [20], or they can be interconnected via various configured interface DC/DC converters [21,22].

Battery is an important energy source of various portable and movable appliances, such as laptop computers and electric vehicles [23-25]. To effectively use battery storage energy, the study of the use of batteries in emergency application for a laptop computer has been presented in [25,26]. The vehicle-to-grid (V2G)/grid-to-vehicle (G2V) operations have also gradually received attention [27-29]. Besides, there are specific battery energy storage systems (BESSs) being developed [30-35]. In addition to the autonomous operation of supplying power to

http://dx.doi.org/10.5772/61248

critical loads [30-32,35], BESSs also possess grid-to-battery charging and battery-to-grid discharging capabilities. The line current in grid-side can also be regulated to be nearly sinusoidal, thanks to its power conditioning control ability. In the studied BESS, its DC-link voltage ($V_{dc}$=400V) is established from the Li-ion battery bank ($v_B$=96V) via an interleaved DC/DC boost-buck converter that has fault-tolerance capability. For effectively utilizing other renewable sources, a plug-in energy harvesting system is developed to make battery supplementary charging from the possible AC and DC sources. As far as the AC source is concerned, a suitable SMR and its control are needed.

In a DC micro-grid or distributed power system, the DC sources and energy storage devices must be interfaced to its common DC-link using suited DC/DC converter [36,37]. For batteries and supercapacitors, bidirectional DC/DC converters are needed to perform charging and discharging operations. For applications with battery voltage being lower than its interfaced DC-link, one can apply the one-leg half-bridge boost-buck bidirectional DC/DC converter [20]. To possess lower current ripples and fault-tolerance capability, the interleaved DC/DC converter [38] can be adopted.

Basically, SMR is formed by inserting a suited DC/DC converter between the diode bridge rectifier and the output filtering capacitor. The surveys for single-phase and three-phase SMRs can be found in [39-43]. For three-phase plants with less stringent power quality requirement, one can adopt the three-phase single-switch (3P1SW) SMR [44,45]. By operating it under discontinuous conduction mode (DCM), the power factor correction is inherently preserved without current feedback control. If higher efficiency is desired, the bridgeless DCM three-phase SMR presented in [35] can be employed. To yield good line drawn current waveform tracking control with the minimum switch number, the three-phase three-switch (3P3SW) Vienna SMR [46,47] is a good choice. However, these two types of SMRs possess only AC-to-DC unidirectional power flow capability. For interfacing the output of a wind AC generator, such as wind permanent-magnet synchronous generator (PMSG), to the common DC-bus in DC micro-grid, a suited AC/DC converter is needed. The de-rated characteristics for various AC/DC followed converters can be found in [48]. From the compromised considerations in switch number, switch voltage stress, conversion loss, operation quadrant number, and control performance, the Vienna rectifier [49-51] with three switches is a better choice to be the interface converter of AC wind generators. On the other hand, the standard three-phase six-switch (3P6SW) SMR [35] should be used for conducting bidirectional power transfer operations.

SMR can directly provide adjustable and well-regulated DC output voltage from the available AC source with good line drawn power quality. This article presents the operation controls and applications of SMRs in micro-grid system incorporating BESS and EV as supplemental facilities. The contents of this article mainly include: (i) Exploration of classifications, operation principle, and some key issues of SMRs; (ii) Functional description of the studied system; (iii) Introduction to the controls and operations of SMRs in micro-grid, wind generators, grid-connected interface power converters, BESS, and EV; (iv) Experimental evaluations for the studied plant in various operation cases.

## 2. System configuration

System configuration of the studied system is shown in Fig. 1. It mainly consists of a grid-connected DC micro-grid, an EV PMSM drive with G2V/V2H/V2G functions, and a grid-connected BESS. The detailed schematics of the constituted plants are shown in Fig. 2. The key system components and features of these three power stages are:

**A. DC Micro-grid**

**a.** Sources: DC source and wind PMSG and their interface converters. For the latter, the advantages of using SMR in de-rated characteristics and generation efficiency enhancements are presented. The other possible harvested AC and DC sources can also be plugged into the system via embedded interface converter schematics.

**b.** Hybrid energy storage system that consists of a battery bank, a super-capacitor (SC) bank, and a PMSM-driven flywheel. Each device is interfaced to the common DC bus via a bidirectional DC-DC boost-buck converter. The output of the flywheel system can be directly connected to the micro-grid common-DC bus for its voltage boosting ability.

**c.** Bidirectional single-phase three-wire (1P3W) load inverter wherein the following operations are allowed: (i) M2G operation: the inverter can power the local load to reduce the power fed from utility. Moreover, the programmed power can be sent back to the utility grid; (ii) G2M operation: the single-phase SMR is formed to allow the utility supply power to the micro-grid for energy supporting or making the battery supplementary charging. The EV can also perform the G2V/V2G operations via its own schematics or via the micro-grid interface converters (G2M+M2V)/(V2M+M2G).

**B. EV PMSM Drive**

The developed battery/SC powered EV IPMSM drive possesses G2V/V2H/V2G operation capabilities. The battery bank and SC bank are integrated to the common DC-link, respectively, via an interleaved and a standard bidirectional front-end DC/DC converter. And the SC bank is connected to the battery bank through a diode to allow the restored regenerative braking energy in SC be charged to battery automatically. Through proper arrangement, the G2V charging and V2H/V2G discharging operations are applicable using the integrated converters and inverters formed by the motor drive embedded components.

In idling G2V operation mode, the battery bank can be charged by the utility grid. A single-phase boost SMR and a three-phase boost SMR are formed to charge the battery bank through the bidirectional interleaved buck DC/DC converter with satisfactory line drawn power quality from the mains. The interconnected operations of the EV to the micro-grid and BESS are also conductible. Moreover, the V2G/G2V via micro-grid or BESS is achievable.

**C. BESS**

The DC-link voltage (400 V) is established from the 96 V battery bank via an interleaved bidirectional interface DC/DC converter with two cells. A multifunctional inverter is established to perform the autonomous and grid-connected operations:

http://dx.doi.org/10.5772/61248

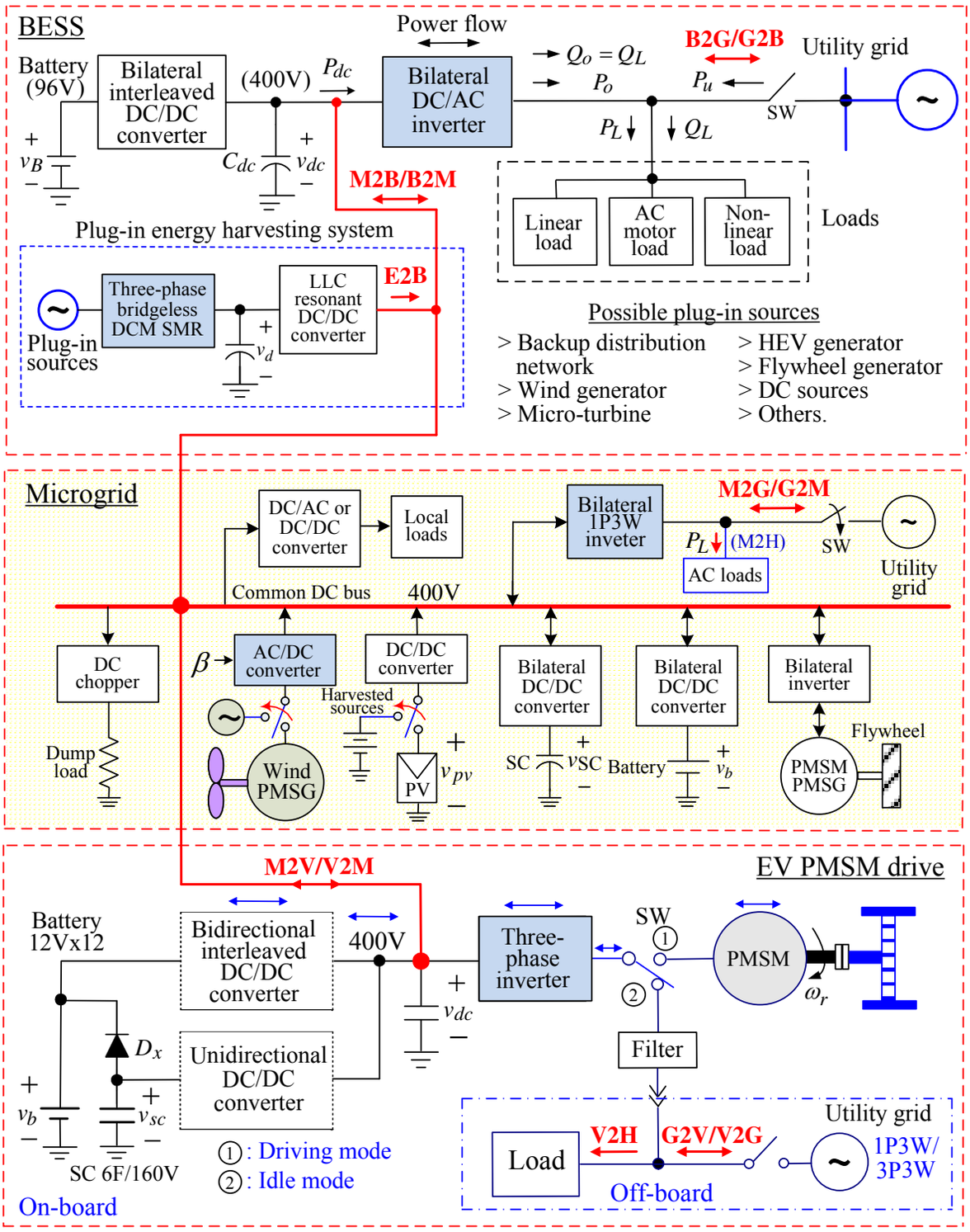


G2V: grid-to-vehicle, V2G: vehicle-to-grid, V2H: vehicle-to-home, M2G: microgrid-to-grid, M2V: microgrid-to-vehicle, V2M: vehicle-to-microgrid, E2B: energy-harvetser-to-BESS, B2G: BESS-to-grid, G2B: grid-to-BESS, M2B: microgrid-to-BESS, B2M: BESS-to-microgrid.

**Figure 1.** System configuration of the studied micro-grid incorporating with EV and BESS.

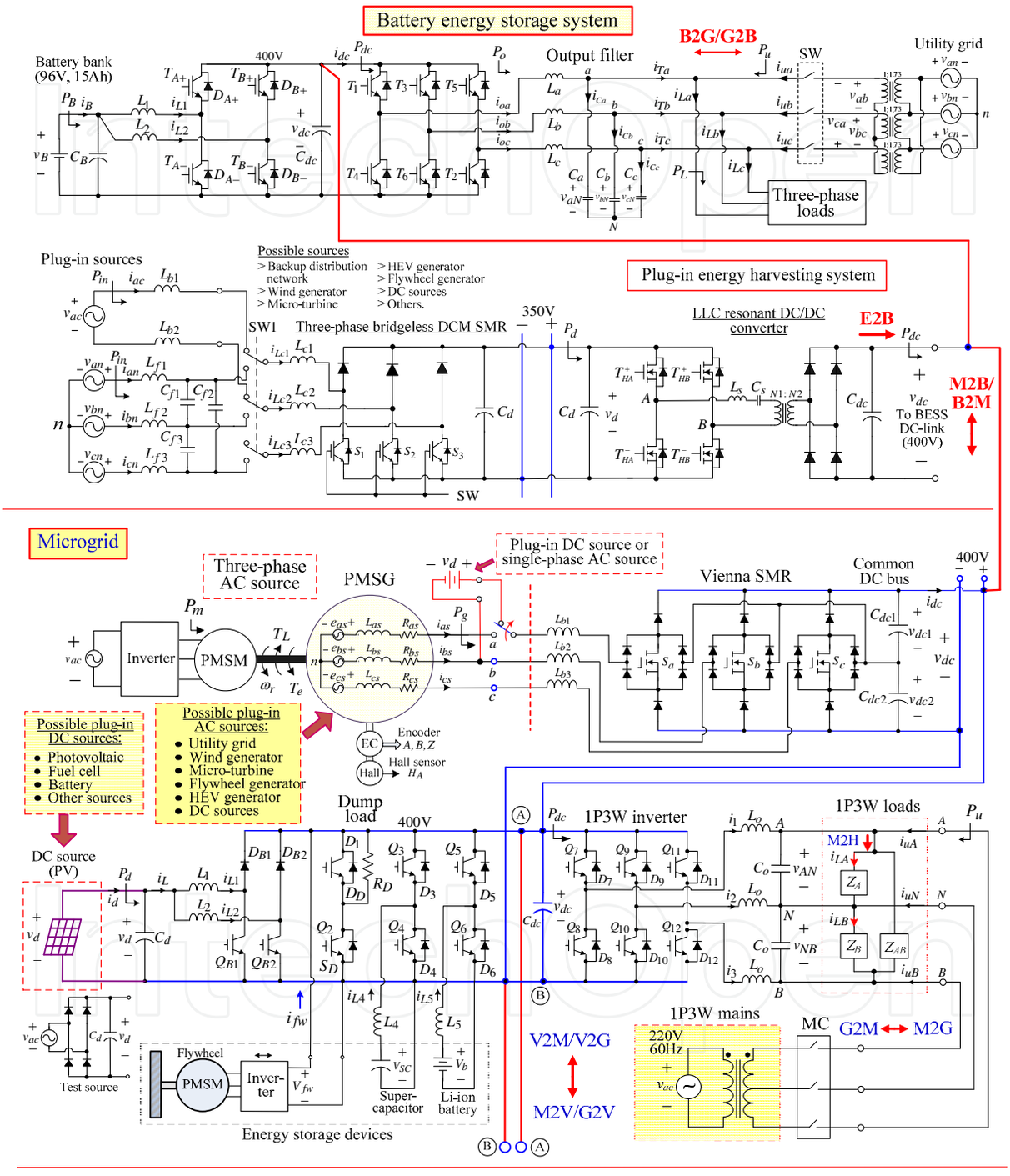
Battery energy storage system
B2G/G2B
Battery bank (96V, 15Ah)
400V
Output filter
SW
Utility grid
Three-phase loads
Plug-in sources
Possible sources
> Backup distribution network
> Wind generator
> Micro-turbine
> HEV generator
> Flywheel generator
> DC sources
> Others.
Plug-in energy harvesting system
SW1
Three-phase bridgeless DCM SMR
350V
LLC resonant DC/DC converter
E2B
M2B/ B2M
To BESS DC-link (400V)
Microgrid
Three-phase AC source
PMSG
Plug-in DC source or single-phase AC source
Vienna SMR
Common DC bus
Possible plug-in DC sources:
Photovoltaic
Fuel cell
Battery
Other sources
Possible plug-in AC sources:
Utility grid
Wind generator
Micro-turbine
Flywheel generator
HEV generator
DC sources
Encoder
Hall sensor
Dump load
1P3W inverter
1P3W loads
DC source (PV)
Test source
Flywheel
Super-capacitor
Li-ion battery
Energy storage devices
1P3W mains
220V 60Hz
MC
G2M
M2G
V2M/V2G
M2V/G2V

(a)

http://dx.doi.org/10.5772/61248

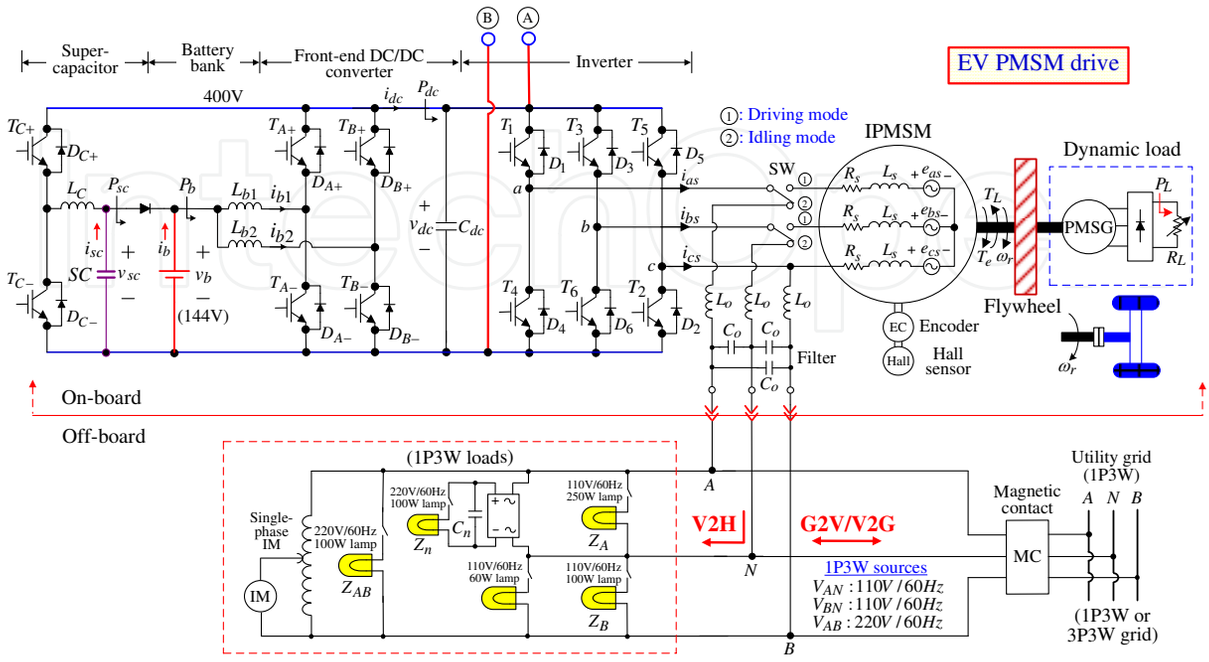


(b)

**Figure 2.** Schematics of all constituted power stages in the studied system: (a) BESS and microgrid; (b) EV PMSMdrive.

**a.** Autonomous operation

The BESS is independent from the utility grid and supplies power to the load.

**b.** Grid-connected operation

The BESS with three-phase six-switch bidirectional inverter can be arranged to operate in three modes: (i) battery-to-grid (B2G) discharging mode: the BESS provides all load powers and sends the preset real power to the utility grid; (ii) grid-to-battery (G2B) charging mode: the utility grid supplies the load real power and also charges the battery bank with good line drawn power quality; (iii) floating mode: all load real powers are supplied by the utility grid. The BESS can compensate all load reactive and harmonic powers under all grid connected operation modes.

The BESS energy can be supported from the possible AC sources and DC sources via the developed plug-in energy harvesting system, i.e., the energy-harvester-to-BESS (E2B) operation mode. Various AC sources and DC sources can be connected to the BESS via the three-phase bridgeless discontinuous current mode (DCM) SMR through proper schematic and control arrangements. Similarly, the interconnected operations of the BESS to the micro-grid and EV are also applicable. Specifically, the EV can be charged by the BESS employing its harvested renewable energies.

## 3. Classification of SMRs

From the viewpoints of schematics and control approaches, the SMRs can be categorized as follows.

### 3.1. Schematics

The SMR schematics can be categorized into: (i) Single-phase or three-phase, the three-phase SMR is a natural choice for the plants with larger ratings; (ii) Non-isolated or isolated, normally, the latter type SMR possesses lower energy conversion efficiency; (iii) Buck, boost, or buck/boost: the boost-type SMR possesses the best PFC control ability since its AC input current is directly related to the energy storage inductor current. As for the buck and buck/boost SMRs, the input low-pass filter is necessary for the inherently discontinuous current; (iv) Single-stage or multi-stage; (v) One-quadrant or multi-quadrant: the multiple quadrant SMR possesses reverse power flow capability from DC side to AC source to achieve the regenerative braking of a SMR-fed AC motor drive; (vi) Hard-switching or soft-switching; (vii) Standard or bridgeless: the bridgeless SMR possesses slightly larger efficiency for the reduced diode voltage drop; (viii) Single-module or interleaved multi-module: the interleaved SMR may have the advantages of rating enlargement, higher reliability owing to redundancy, and smaller current and voltage ripples.

### 3.2. Control methods

**a.** Low-frequency control: for the single-phase boost SMR, only v-loop is needed and only one switching per half AC cycle is applied. It is simple but subject to having limited power quality characteristics.

**b.** High-frequency voltage-follower control: without current control loop, only some specific SMRs operating in DCM possess this feature; see for example, the standard buck-boost SMR and the flyback SMR.

**c.** High-frequency standard control: it belongs to multiplier-based current-mode control scheme with cascade v- and i-control loops.

## 4. Single-Phase SMRs

### 4.1. Operation and schematics

For a properly designed single-phase SMR, the AC input current $i_{ac}$ can be regulated to be sinusoidal and kept in phase with $v_{ac}$, then the SMR can be regarded as an emulated resistor with the effective resistance of $R_e$ viewing from the utility grid. However, the double line frequency output voltage ripple always exists. It can be derived to obtain the peak to peak value of output ripple voltage:

$$\Delta v_{dc} = \frac{V_{dc}}{\omega\, C_{dc} R_{dc}} \tag{1}$$

where $R_{dc}$= equivalent DC load resistance, $\omega = 2\pi f_1$ and $f_1$=60Hz.

In reality, the operation characteristics of an SMR including DC output voltage and AC input power quality are highly affected by the energy storage inductor current PWM control behavior.

Figs. 3(a) to 3(e) show some typical single-phase boost SMR circuits, including: (a) standard type SMR; (b) bridgeless SMR: its efficiency is increased by reducing one diode voltage drop in each half AC cycle; (c) curret-fed push-pull (CFPP) isolated SMR: the higher voltage boosting ratio is obtained by the duty ratio control and the turn ratio; (d) zero-voltage transition (ZVT) soft-switching SMR: the ZVT soft switching is achieved by adding an auxiliary resonant branch [52]; (e) four-quadrant SMR: the H-bridge converter based SMR possesses four operation quadrants. A bidirectional battery energy storage system [25] is shown in Fig. 3(e)

The single-phase standard buck SMR is depicted in Fig. 4(a), the input filter is needed for its discontinuous input current. The power factor will become worse for the higher output DC voltage. Figs. 4(b) to 4(c) correspond to the standard, the Cuk continuous, and the flyback isolated buck/boost SMRs, respectively. Except for the Cuk SMR, the input filtering is still necessary for the other two types of buck/boost SMRs. In control aspect, the simple voltage-follower control scheme can be applied for these buck/boost SMRs operated in DCM.

### 4.2. Some key issues

Some key issues for a boost SMR and a buck/boost SMR are indicated in Fig. 5 and Fig. 6. Some comments are given as:

**a.** The input filter is needed for buck/boost SMRs due to the discontinuous input current.

**b.** The ripples and ratings of the power circuit constituted components must be properly designed and implemented.

**c.** For the boost SMR in CCM operation, the standard cascade multiplier-based control scheme with v and i loops must be adopted.

**d.** The voltage follower control scheme without inner current loop can be applied for the buck/boost SMR in DCM operation owing to its inherent PFC capability.

**e.** In treating the control affairs, the sensed inductor current and output voltage should be filtered with suited low-pass cut-off frequencies. The feedack controller must first be properly designed considering the desired transient and static performances and the effects of comtaminated noises in sensed variables. Normally, the voltage dynamic response speed is: << ($2f_1$=120Hz), whereas the inner current dynamic response is set as: << switching frequency, but >> ($2f_1$=120Hz).

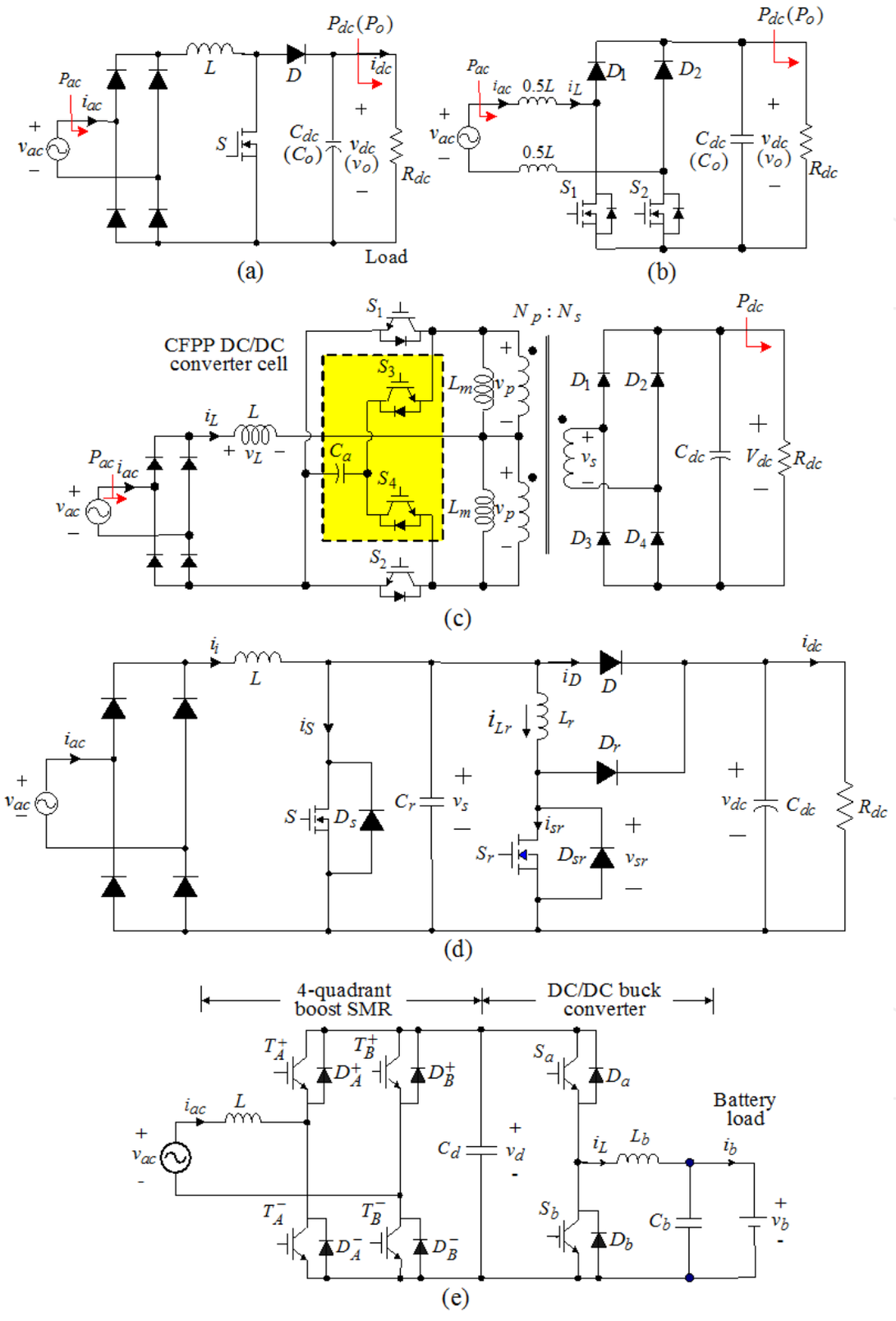


**Figure 3.** Some typical single-phase boost SMR circuits: (a) standard SMR; (b) bridgeless SMR; (c) CFPP isolated SMR; (d) ZVT soft-switching SMR; (e) four-quadrant SMR.

http://dx.doi.org/10.5772/61248

## 5. Three-phase SMRs

### 5.1. Operation and schematics

Detailed surveys for the existing three-phase SMR circuits can be referred to [41-43]. The complexities of schematic and control mechanism depend on the control ability and the desired performances. Some commonly used three-phase boost SMRs shown in Figs. 7(a) to 7(e) include:

**a.** Three-phase, single-switch (3P1SW) DCM SMR (Fig. 7(a)): by operating it in DCM, the PFC is naturally preserved without applying current PWM control. However, it possesses the following limiations: (i) Having higher input peak current and switch stress; (ii) The input line current contains significant lower-frequency harmonics with the orders of 6n ±1, n=1, 2,..., and the dominant ones are the 5th and 7th harmonics. Thus, suitably designed AC-side, low-pass filter is required to yield satisfactory power quality; (iii) The line drawn power quality is limited, typically the power factor is slightly higher than 0.95; (iv) It possesses only one-quadrant capability.

**b.** Bridgeless, three-phase DCM SMR: As shown in Fig. 7(b) [35], one diode drop is eliminated in each line-current path to increase the efficiency compared to 3P1SW SMR.

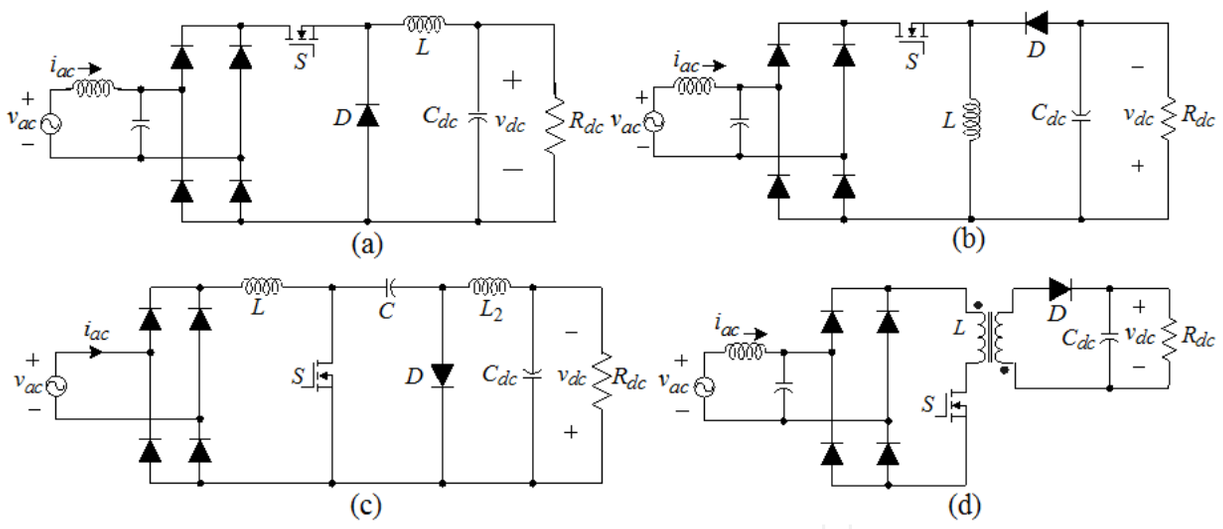


**Figure 4.** Some typical single-phase buck and buck/boost SMR circuits: (a) standard buck SMR; (b) standard buck/boost SMR; (c) Cuk buck/boost SMR; (d) flyback isolated SMR.

**c.** Three-phase Vienna SMR [46,47] (Fig. 7(c)): it uses only three switches to achieve good current command tracking control. It can be regarded as a simplified version of three single-phase PFCs connected to the same intermediate bus voltage. The major features of this SMR are: (i) three output voltage levels ($0.5v_o$, $v_o$, $-0.5v_o$) providing larger switching control flexibility; (ii) lower switch voltage rating of, $0.5\ v_o$ rather than $v_0$ ; and (iii) lower input current distortion. However, it has only unidirectional power flow capability, and

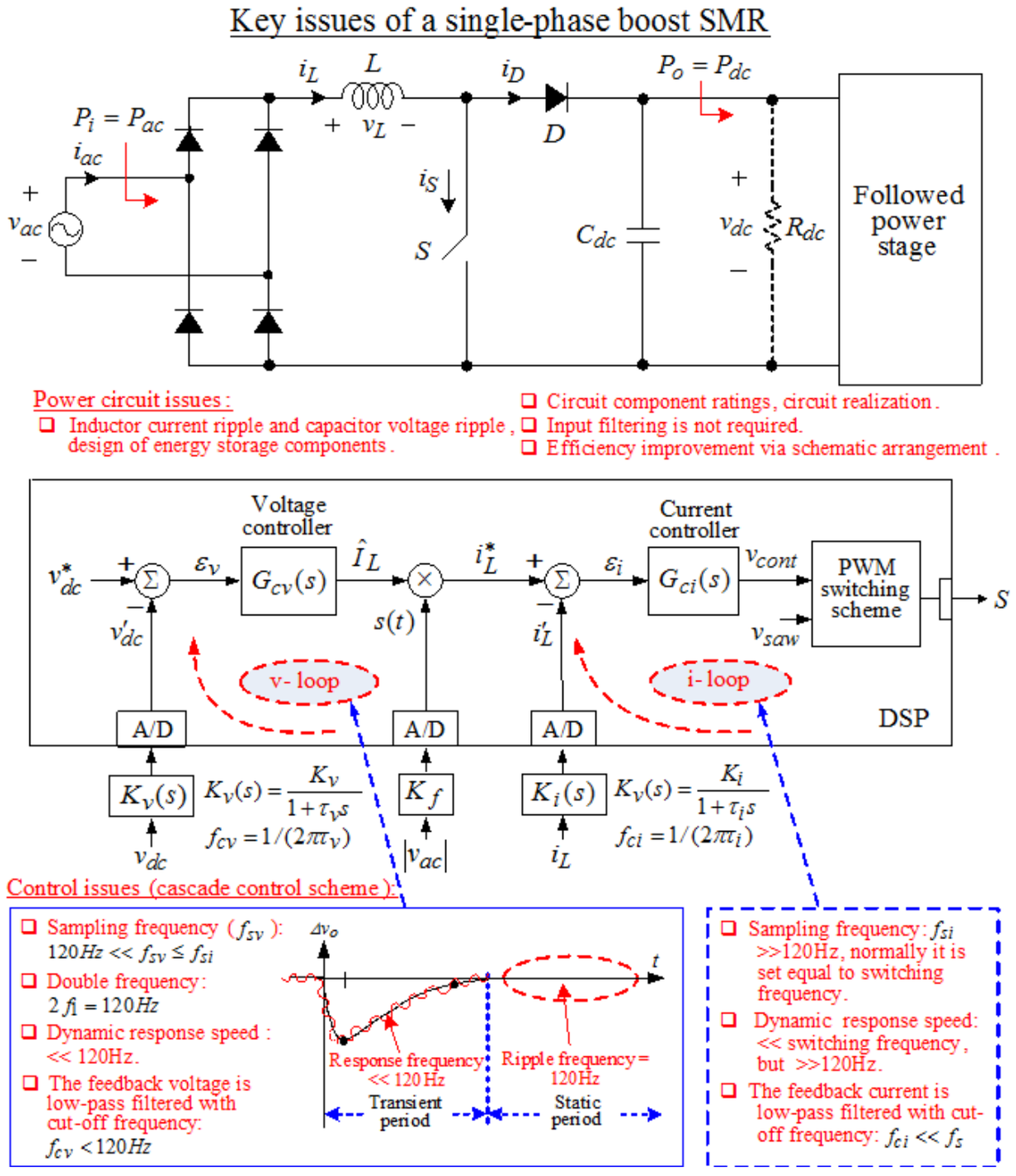


**Figure 5.** Some key issues of single-phase boost SMRs.

needs a complicated power switch and two serially connected capacitors. The specific power switch (VUM 25-05) for implementing this SMR is available from IXYS Corporation, USA.

**d.** Three-phase six-switch standard SMR (Fig. 7(d)): the standard three-phase six-switch SMR [41,42] possesses four operation quadrants and high flexibility in power conditioning

http://dx.doi.org/10.5772/61248

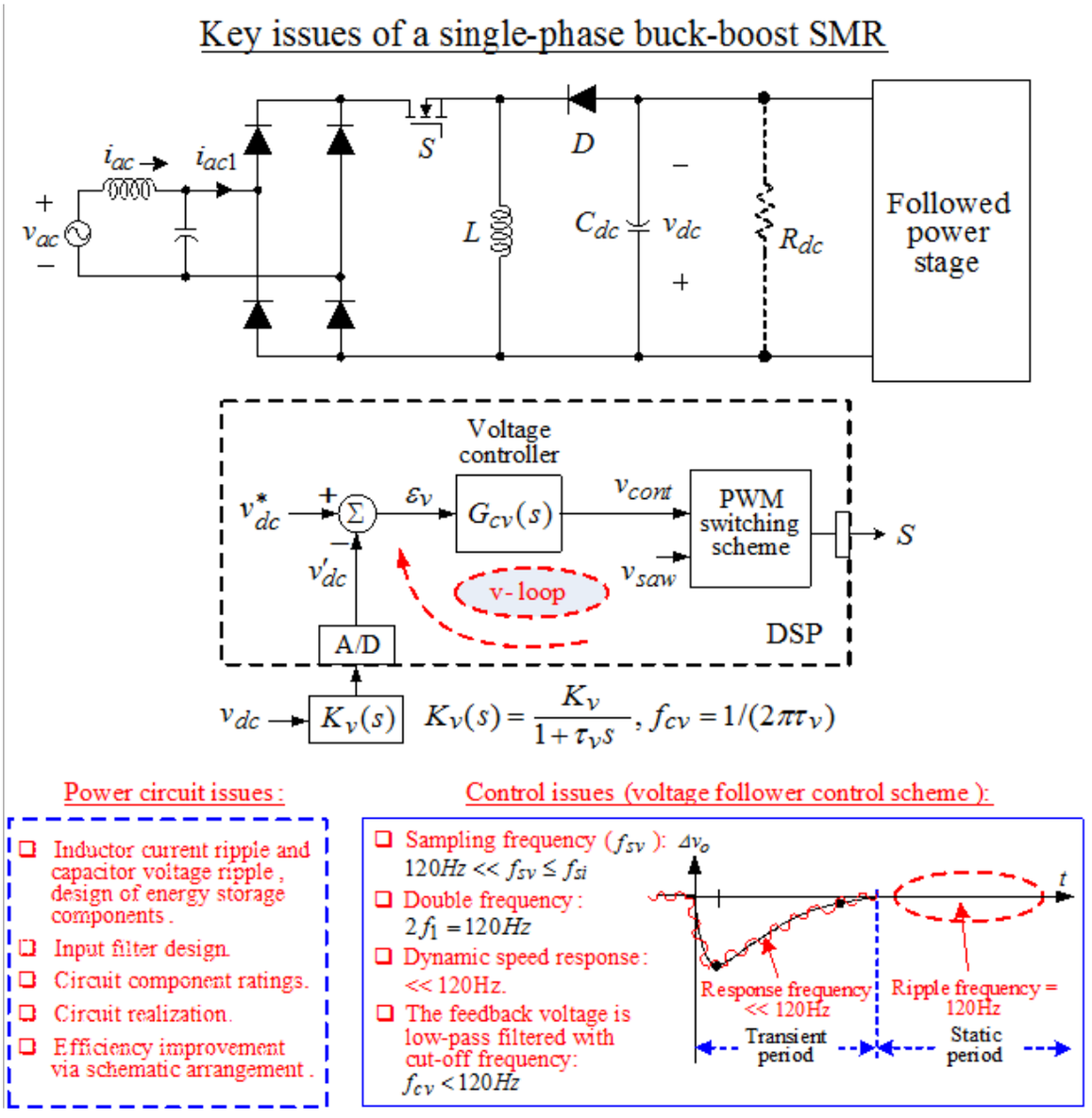


**Figure 6.** Some key issues of single-phase buck/boost SMRs.

control. For a motor drive equipped with such SMR, it may possess regenerative braking ability. However, the switch utilization ratio of this SMR is low, and its control is complicated.

**e.** Neutral-point clamped (NPC) three-phase standard SMR: the three-level NPC three-phase SMR is shown in Fig. 7(e) where the voltage ratings of its constituted power switches and diodes can be only one-half of the DC-link voltage, rather than the full voltage for the standard SMR shown in Fig. 7(d).

**Three-phase single-switch (3P1SW) DCM SMR:**

For a well-regulated three-phase single-switch (3P1SW) DCM SMR shown in Fig. 7(a), it can be regarded as a loss-free emulated resistor $R_e$ viewing from the phase AC source with line

drawn current having dominant 5th and 7th harmonics [44]. Hence, the three-phase line drawn instantaneous power can be approximately expressed as:

$$\begin{aligned} p_{ac} &= v_{an}i_a + v_{bn}i_b + v_{cn}i_c = \frac{V_m^2 \sin\omega t}{R_e}\left[\sin\omega t - \frac{1}{5}\sin 5\omega t - \frac{1}{7}\sin 7\omega t\right] + \\ &\frac{V_m^2 \sin\left(\omega t - 2\pi/3\right)}{R_e}\left[\sin\left(\omega t - 2\pi/3\right) - \frac{1}{5}\sin 5\left(\omega t - 2\pi/3\right) - \frac{1}{7}\sin 7\left(\omega t - 2\pi/3\right)\right] + \\ &\frac{V_m^2 \sin\left(\omega t + 2\pi/3\right)}{R_e}\left[\sin\left(\omega t + 2\pi/3\right) - \frac{1}{5}\sin 5\left(\omega t + 2\pi/3\right) - \frac{1}{7}\sin 7\left(\omega t + 2\pi/3\right)\right] \\ &= \frac{3V_m^2}{2R_e} + \frac{3V_m^2}{35R_e}\cos 6\omega t \triangleq P_{ac} + \delta p_{ac} \end{aligned} \tag{2}$$

where $\delta p_{ac}$ = ripple AC power and the average AC power $P_{ac}$ is:

$$P_{ac} = \frac{3V_m^2}{2R_e} = \frac{V_{dc}^2}{R_{dc}} \tag{3}$$

The AC charging current flowing the output filtering capacitor is:

$$C_{dc}\frac{dv_{dc}}{dt} = \frac{2V_{dc}}{35R_{dc}}\cos 6\omega t \tag{4}$$

Thus, one can derive the peak-to-peak output voltage ripple from (4):

$$\Delta v_{dc} = \frac{2V_{dc}}{105\omega R_{dc}C_{dc}} \tag{5}$$

**Three-phase Vienna SMR and three-phase six-switch standard SMR:**

For the Vienna SMR and three-phase six-switch standard SMR with satisfactory current mode control, the three-phase line drawn currents will be balanced without harmonics. Hence, from (2) one can find that the DC output voltage ripple will be nearly zero.

### 5.2. Derated characteristics of a PMSG followed by different AC-DC converters

The total derate factor of a surface-mounted PMSG (SPMSG) and an interior PMSG (IPMSG) followed by various AC-DC converters can be derived to be [48]:

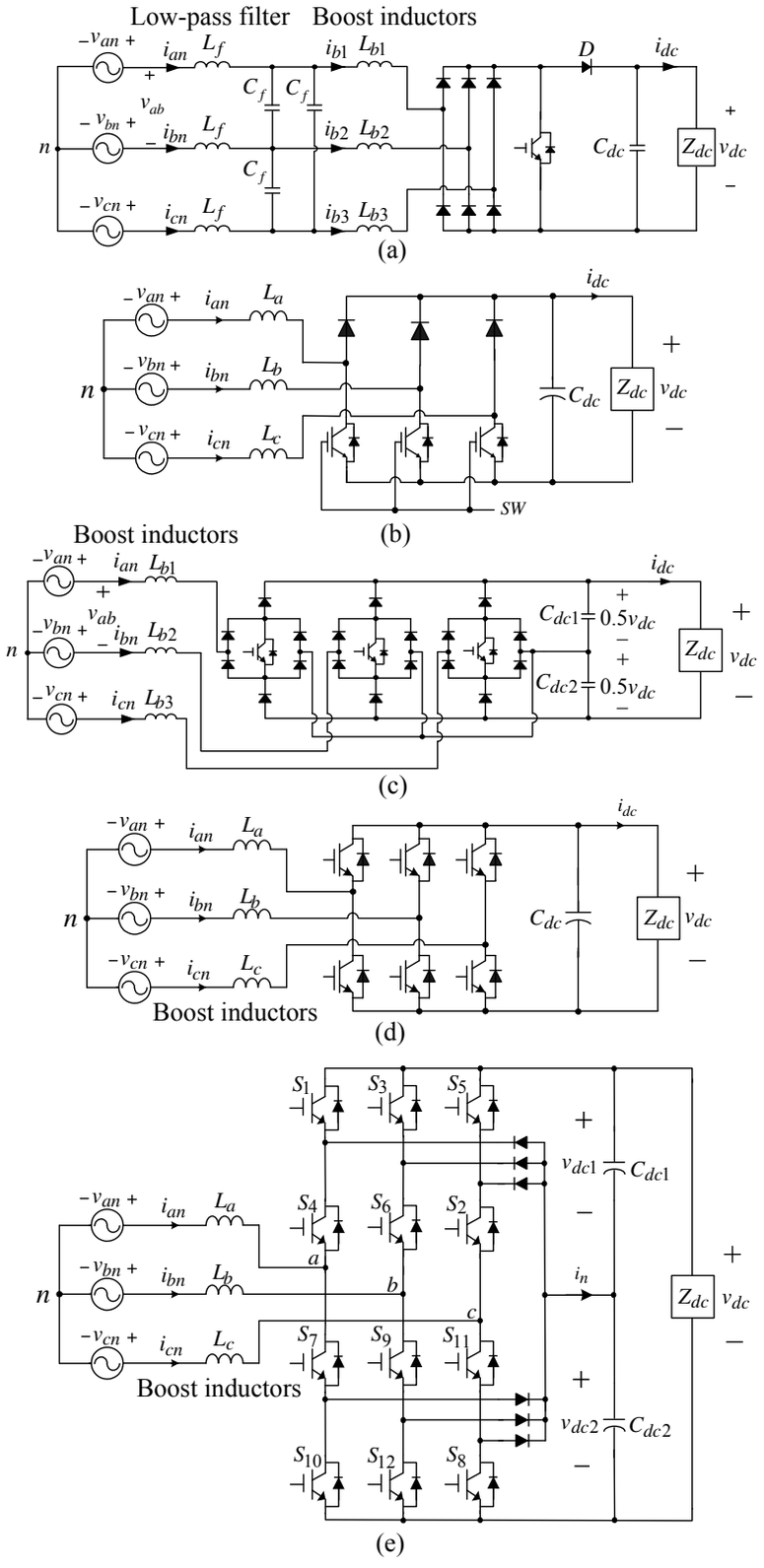


**Figure 7.** Some typical three-phase boost SMR circuits: (a) 3P1SW SMR; (b) Bridgeless three-phase DCM SMR; (c) Three-phase Vienna SMR; (d) Three-phase six-switch standard SMR; (e) NPC three-phase standard SMR.

$$DF \overset{\Delta}{=} (DF_1)(DF_2) = \begin{cases} (DF_1)\cos\delta & \text{for SPMSG} \\ (DF_1)\cos\delta\left(\dfrac{P_f}{P_f + P_r}\right) & \text{for IPMSG} \end{cases} \tag{6}$$

$$DF_1 \overset{\Delta}{=} \frac{I_{as1}}{I_{as}} = \frac{1}{\left(1 + THD_i^2\right)^{0.5}} \tag{7}$$

$$DF_2 = \cos\delta\frac{P_f}{P_e} = \cos\delta\frac{P_f}{P_f + P_r} \tag{8}$$

where, $I_{as}$ = rms value of armature phase current $i_{as}$, $I_{as1}$ = rms value of fundamtal armature phase current $i_{as1}$, $THD_i$ = total harmonic distortion of $i_{as}$, $\delta$ = the power angle between the back-EMF $e_{as}$ and the terminal voltage $v_{as}$, $P_e$ = electromagnetic developed power, $P_f$ = magnetic field developed power, $P_r$ = reluctance developed power.

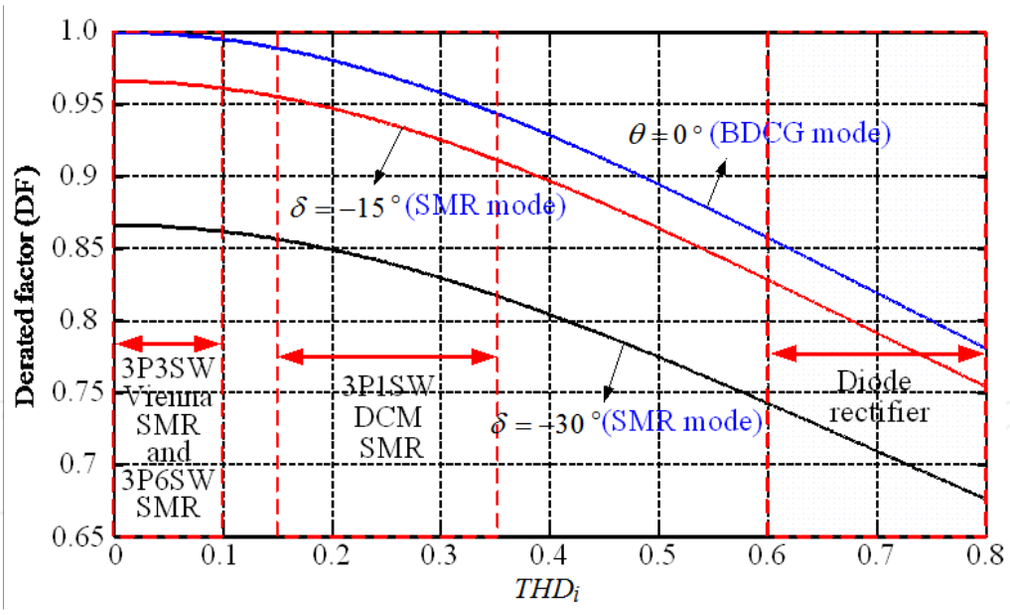


**Figure 8.** The de-rated characteristics of a PMSG with various AC-DC followed converters and operation control modes.

The de-rated characteristics of a wind PMSG followed by various AC-DC converters and operation control modes are shown in Fig. 8. Obviously, the conventional diode rectifier possesses significant derate. The three-phase Vienna SMR is a good candidate for being the followed interface converter of the PMSG from the following compromised considerations: (i)

http://dx.doi.org/10.5772/61248

minimum switch number; (ii) winding current PWM control ability; (iii) the commutation shift control ability for an IPMSG; and (iv) only one operation quadrant is required.

## 6. SMR operations and performances

### 6.1. Wind IPMSG based micro-grid

In the developed wind IPMSG-based DC micro-grid shown in Fig. 2, its common DC bus voltage $v_{dc}$=400V is established by the interleaved DC/DC boost converter from the possible harvested DC sources (here a DC power supply with $v_d$=35V is used as a substitute), and also by the plug-in Vienna switch-mode rectifier (SMR) from the wind PMSG or other possible harvested AC sources. The equipped hybrid energy storage system consists of battery/SC/flywheel. The M2G/G2M operations can be made by the developed 1P3W inverter. The micro-grid incorporating with EV can allow the V2G/G2V operations to be applicable via the 1P3W inverter in the established micro-grid. The EV on-board battery can supply power to the micro-grid local loads, and even send the programmed power back to the utility grid.

**A. System Components**

**1.** AC source: wind IPMSG followed by Vienna SMR

- IPMSG: 1 kW, 3.23 N-m, 3,000 rpm, 4.8 A. An SPMSM (2 kW, 9.8 N-m, 2,000 rpm, 9.6 A) is served as the prime mover for driving the IPMSG.
- Vienna SMR:
- $L_{b1}$=3.28mH/60Hz, $L_{b2}$=3.28mH/60Hz, $L_{b3}$=3.29mH/60Hz, $C_{dc1}=C_{dc2}$=2200$\mu$F/400V
- Possible plug-in sources: Various harvested AC and DC sources as indicated in Fig. 1 can be plugged into the micro-grid via the input of the Vienna SMR.

**2.** DC source interleaved DC-DC boost converter

- $v_d$=35V, $v_{dc}$=400V, $P_{dc}$=1kW.
- $L_1$=2.17mH/30kHz, $L_2$=2.16mH/30kHz, $C_d$=100$\mu$F/400V
- Possible plug-in DC sources: Photovoltaic, fuel cell, battery, or other possible harvested sources. A DC source is employed here as an alternative.

**3.** Storage device interface DC-DC converters

- Battery: 96 V/15 Ah; SC bank: 96 V/40 F; SPMSM driven flywheel: 2 kW, 2,000 rpm, $J$ = 0.9263 (kg-m2).
- $L_4$=965.7$\mu$H, $L_5$=947.3$\mu$H/30kHz, $C_{dc}$=2200$\mu$F/450V.

**4.** 1P3W load inverter

It can yield the 220 V/110 V AC voltages for powering the domestic appliances and performing the M2G/G2M bidirectional operations.

- AC output: 220 V/110 V 60 Hz, 1 kW.
- $L_o$=401.62$\mu$H/30kHz, $C_o$=10$\mu F$ /400VAC.

**5.** Dump load: $R_D$=36Ω/2kW

**B. Control Schemes**

In the DC micro-grid shown in Fig. 2, the control scheme of the wind IPMSG with followed Vienna SMR is shown in Fig. 9(a), and the differential mode (DM) and common mode (CM) control schemes of the 1P3W inverter are depicted in Fig. 9(b). The detailed design description is being neglected here. The designed controllers are [51]:

**1.** Wind IPMSG followed Vienna SMR

$$G_{cv}(s) = 4.5 + \frac{675}{s},\ W_v(s) = \frac{W_v}{1+\tau_v s} = \frac{0.6}{1+1.59\times10^{-3}s}$$
$$G_{ci}(s) = 4 + \frac{6000}{s},\ W_i(s) = \frac{W_i}{1+\tau_i s} = \frac{0.3}{1+1.59\times10^{-4}s}$$

**2.** 1P3W inverter G2M SMR charging mode: The micro-grid can be supported energy from the mains via the SMR formed using the power devices of the 1P3W inverter with power factor correction by the control scheme as shown in Fig. 9(b). The single-phase SMR with 220V/60Hz input is formed by ($Q_7$, $Q_8$, $Q_{11}$, $Q_{12}$). The predictive current control is applied to yield fast tracking response. And the voltage and active power controller are set as:

$$G_{cv}(s) = 0.1 + \frac{2.5}{s},\ G_{apc}(s) = 5 + \frac{150}{s},\ LPF: H_{LP}(s) = \frac{1}{1+1.591\times10^{-2}s}$$

By properly selecting the current magnitude command $\hat{I}_{as}$ and the commutation shift angle $\beta$, the developed IPMSG with Vienna SMR can be operated in voltage control mode ($\hat{I}_{as}=\hat{I}_{asv}$, $\beta=\beta_v$) and in MPPT control mode for a wind generator ($\hat{I}_{as}=\hat{I}_{asw}$, $\beta=\beta_w$).

**C. Experimental Results**

**a.** IPMSG with followed Vienna SMR

Using the estimated parameters of the IPMSG and the given torque command $T_e$ from the wind power MPPT control mechanism, the relationship of its phase current magnitude command $\hat{I}_{asw}$ and the commutation shift angle $\beta_w$ can be found [51]. The developed wind generator torque command is preset as $T_e$=3.23(N−m), and the corresponding optimal variables found are ($\beta_w$, $\hat{I}_{asw}$)=(−7.8 , 5.7A). The measured steady state ($v_{dc}$, $\theta_r$, $\hat{\theta}_r$, $i_{as}$) at

http://dx.doi.org/10.5772/61248

($\omega_r$=2000rpm, $R_{dc}$=200Ω) and $\hat{I}_{asw}$=5.7A under ($\beta_w$=−7.8 and $\beta_w$=0 ) are compared in Figs. 10(a) and 10(b), wherein $\hat{\theta}_r=\theta_r+\beta$ denotes the shifted rotor angular position for making current PWM switching control. The measured DC-bus voltages $v_{dc}$ under four $\beta_w$ values are ($\beta_w$=−15 , $v_{dc}$=372.1V), ($\beta_w$=−7.8 , $v_{dc}$=374.3V), ($\beta_w$=0 , $v_{dc}$=369.6V), ($\beta_w$=15 , $v_{dc}$=355.8V). The results indicate that $\beta_w$=−7.8 yields the highest value of $v_{dc}$(=374.3V). This implies that the MPPA for the wind IPMSG with followed Vienna SMR can be achieved. Good IPMSG armature current waveforms are also observed.

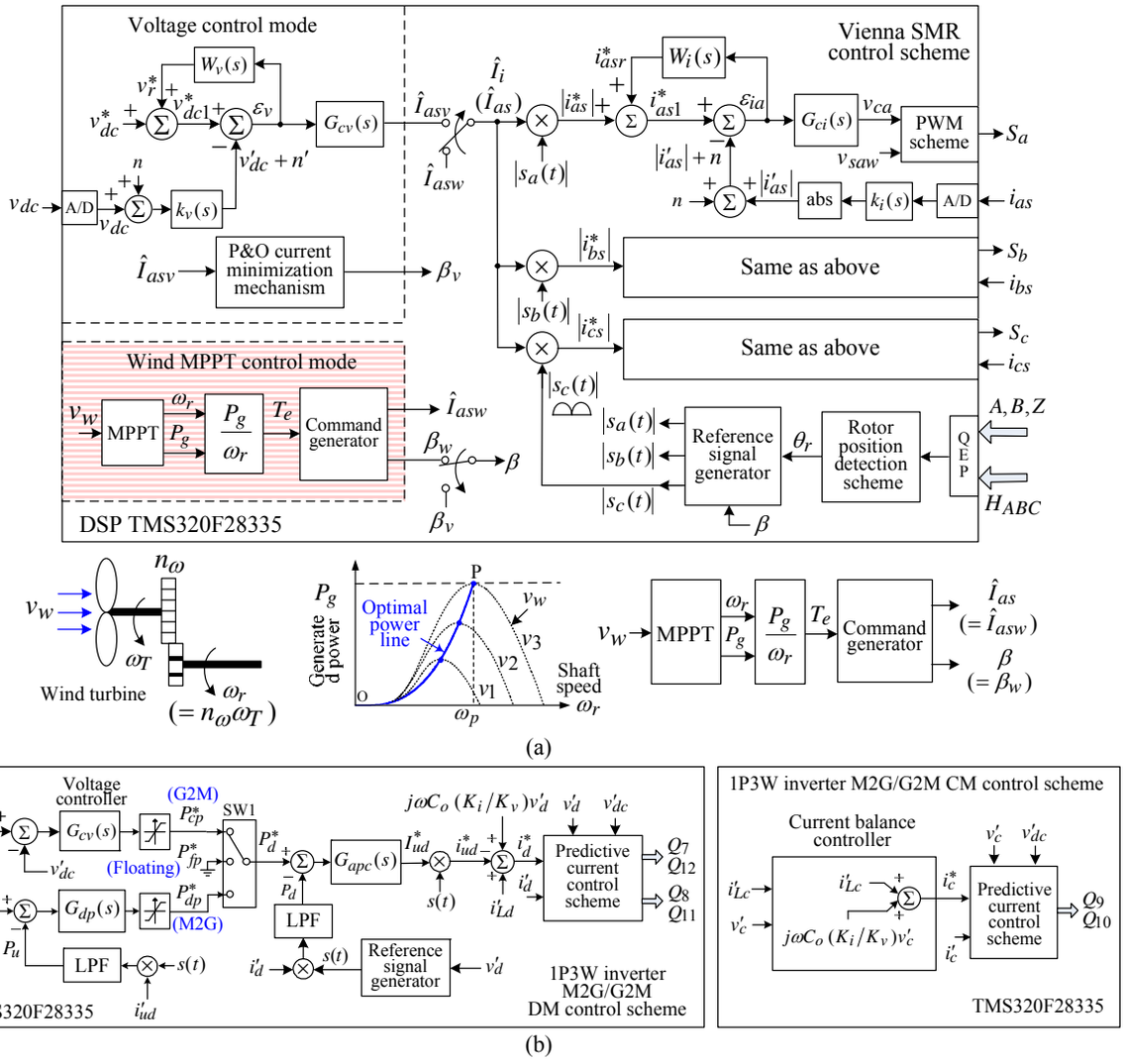


**Figure 9.** Control schemes of the developed wind IPMSG based DC micro-grid system: (a) IPMSG with followed Vienna SMR; (b) DM and CM control schemes of 1P3W inverter in M2G/G2M modes.

**b.** Inter-connected operation between EV IPMSM drive, micro-grid, and utility grid-G2V via micro-grid:

The grid-connected micro-grid is connected to the DC-link of the EV, and the 1P3W inverter load resistors in Fig. 2 are set as ($Z_A$=201.7Ω, $Z_B$=201.7Ω, $Z_{AB}$=484Ω). Let the EV on-board battery be charged from the mains (G2V) via the micro-grid and the EV interfaced DC/DC converter. Figs. 11(a) to 11(c) show the measured EV, micro-grid and grid variables. Good operation performances and line drawn power quality can be observed from the measured results.

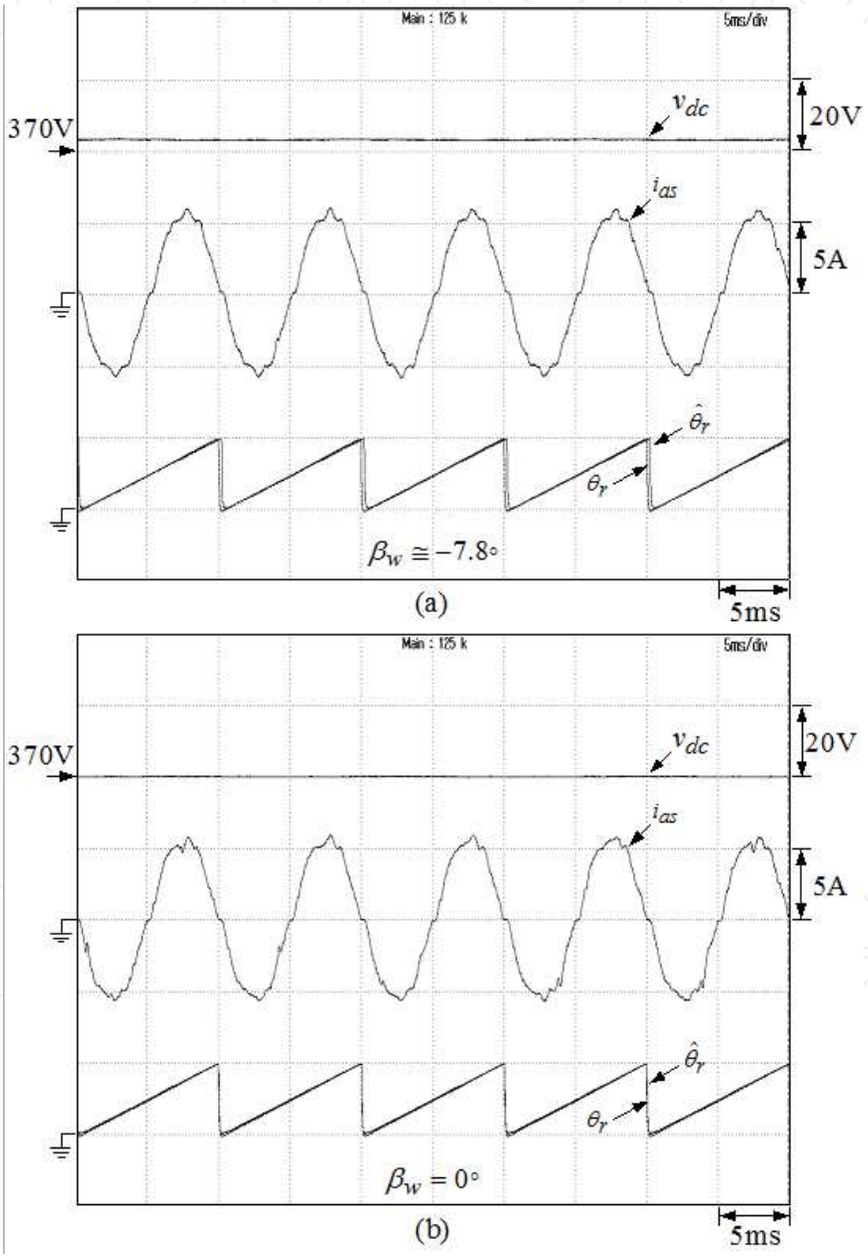


**Figure 10.** Measured steady state ($v_{dc}$, $\theta_r$, $\hat{\theta}_r$, $i_{as}$) of the wind IPMSG with Vienna SMR at ($\omega_r$=2000rpm, $R_{dc}$=200Ω and $\hat{I}_{asw}$=5.7A) under: (a) $\beta_w \cong -7.8$ ; (b) $\beta_w$=0 .

http://dx.doi.org/10.5772/61248

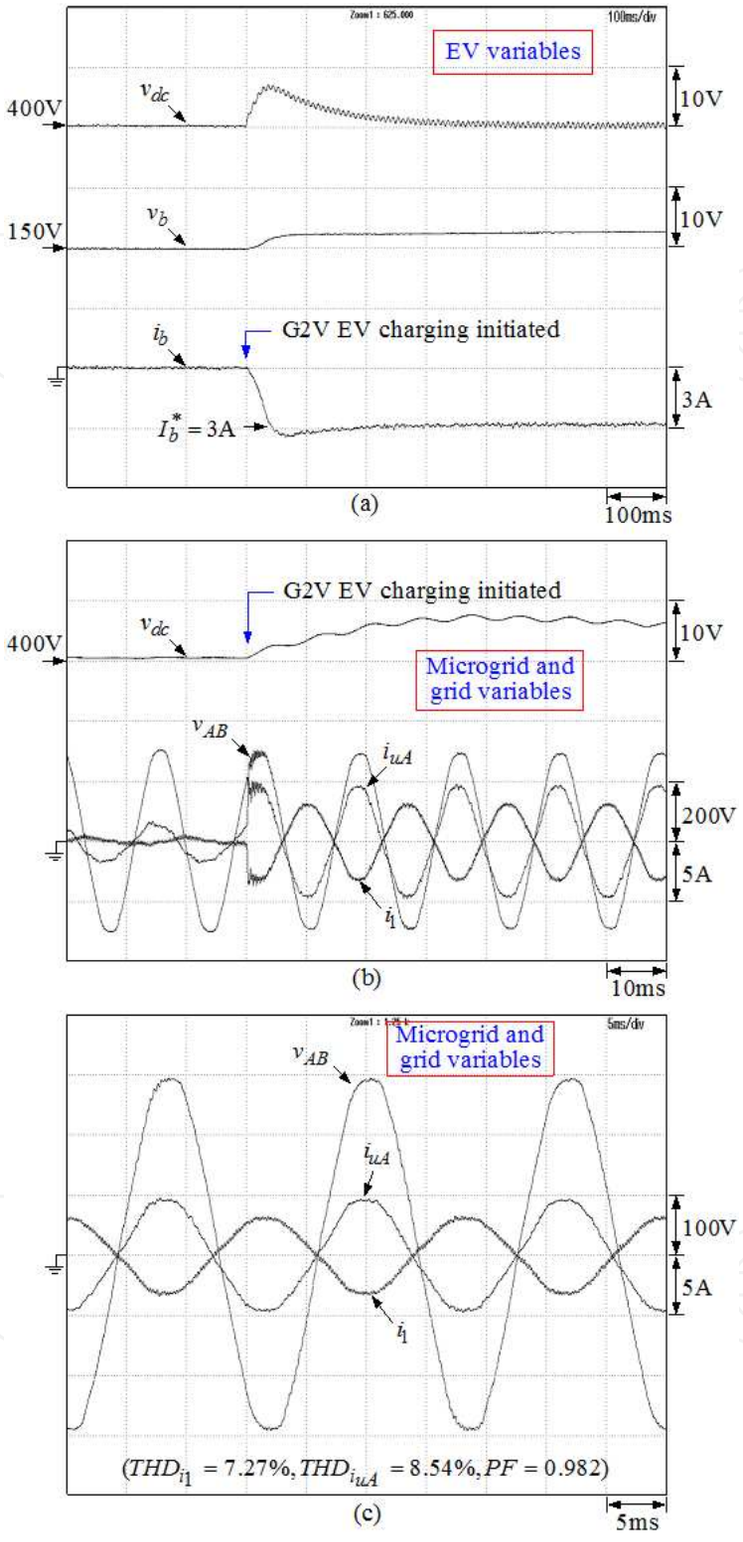


**Figure 11.** Measured results for EV battery charging ($I_b^*$=3A) from the mains (G2V) via the micro-grid at resistive loads of ($Z_A$=201.7Ω, $Z_B$=201.7Ω and $Z_{AB}$=484Ω): (a) dynamic responses of $(v_{dc}, v_b, i_b)$ ; (b) dynamic responses of $(v_{dc}, v_{AB}, i_{uA}, i_1)$ ; (c) steady-state waveforms of $(v_{AB}, i_{uA}, i_1)$.

### 6.2. Grid-connected BESS

The system configuration and schematic of the developed grid-connected BESS is shown in Figs. 1 and 2. It can be operated under floating, discharging, and charging modes. All load reactive and harmonic powers can be compensated by the BESS. In charging mode, the bidirectional inverter is operated in SMR mode to let the BESS be supported energy from the grid (G2B).

In addition, a plug-in energy harvesting system is also equipped for the grid-connected BESS. The harvested AC and DC sources can be inputted to the system via a three-phase bridgeless DCM SMR to establish a 350 V DC-link. Then, it is connected to the developed BESS common DC-link (400 V) via a LLC resonant DC/DC isolated converter.

**A. System Components**

The constituted system parameters are listed below:

**a.** Interleaved DC/DC converter

- **i.** Battery bank voltage: $v_B$=96~105.6V
- **ii.** DC-link: $V_{dc}$=400V (nominal), $C_{dc}$=6400μF/450V
- **iii.** Storage energy inductor: $L_1$=$L_2$=1.74mH/30kHz
- **iv.** IGBT: STGW35NC60WD by STMicroelectronics Company

**b.** Grid-connected inverter

- **i.** Isolation transformer: Y-Δ connected using three single-phase transformers of 60Hz, 127 V/220 V (1/1.73), 1 kVA
- **ii.** Inverter output filter: $L$ =1.71mH/30kHz, $C$=3.3μF/400V
- **iii.** IGBT: STGW35NC60WD by STMicroelectronics company
- **iv.** Inverter output: 3$\varphi$ AC, $v_{ab}$ = 220V/60Hz, 2kW
- **v.** Utility grid: 3$\varphi$ AC, $v_{ab}$ = 220V/60Hz

**c.** Plug-in energy harvesting system

- **i.** Storage energy inductors (at 20kHz): $L_{c1}$=41.12μH, $L_{c2}$=40.95μH, $L_{c3}$=41.55μH
- **ii.** DC-link: $V_d$=350V (nominal), $C_d$=2200μF/500V
- **iii.** Power devices: IGBT: MG100J2YS50 by Toshiba Semiconductor; Diode: fast diode IXYS DSEP 2x-61-12A

**B. Control Schemes**

Fig. 12(a) shows the control schemes of the BESS in charging mode including the battery interface interleaved DC/DC converter and the bidirectional grid-connected three-phase

http://dx.doi.org/10.5772/61248

inverter. Figs. 12(b) and 12(c) are the control schemes of the 3P1SW SMR and LLC resonant DC/DC converter in the developed plug-in energy harvesting system.

**a.** Bidirectional DC/DC interleaved converter

The current and voltage feedback controllers under discharging and charging modes are:

**1.** Discharging mode

$$G_{ci}(s) = K_{Pi} + \frac{K_{Ii}}{s} = 3 + \frac{10}{s},\ G_{cv}(s) = K_{Pv} + \frac{K_{Iv}}{s} = 1.2 + \frac{21.6}{s}$$

**2.** Charging mode

$$G_{ci}(s) = K_{Pi} + \frac{K_{Ii}}{s} = 4.2 + \frac{500}{s},\ G_{cv}(s) = K_{Pv} + \frac{K_{Iv}}{s} = 3 + \frac{90}{s}$$

**b.** Grid-connected inverter

**1.** Current feedback controller: $G_{cbi}(s)=4.5$

**2.** Disturbance and command feed-forward controllers:

$$G'_{dfi}(s) = 1.333,\ G''_{fdi}(s) = \frac{1.133\times10^{-4}s}{(1+5.305\times10^{-4}s)} + 0.603,\ G_{cfi}(s) = \frac{1.133\times10^{-4}s}{(1+5.305\times10^{-5}s)}$$

**3.** Active power controller: $G_{pc}(s)=3+\frac{135}{s}$

**4.** Charging mode controller: $G_{cp}(s)=3+\frac{150}{s}$

**C. Experimental Results**

**a.** BESS battery charging from grid (G2B)

In making the test, the local loads in BESS are set as linear resistive and motor reactive loads with: ($R_a=R_b=R_c=104\Omega$), AC motor with ($V_{IM}=110V_{rms}$). The utility grid supplies the local load real power and also charges the battery bank. The inverter establishes the 400V DC link and also compensates reactive and harmonic powers of local loads. The battery bank charging is conducted via the bidirectional interface DC/DC converter in buck mode. Initially, the battery is charged under constant current mode with $I_B$=5A(0.33C) until the voltage is raised to 114 V, then the constant voltage floating charging is applied instead. The measured results are shown in Figs. 13(a) and 13(b). Satisfactory line drawn current waveform and power quailty can be observed from the measured results.

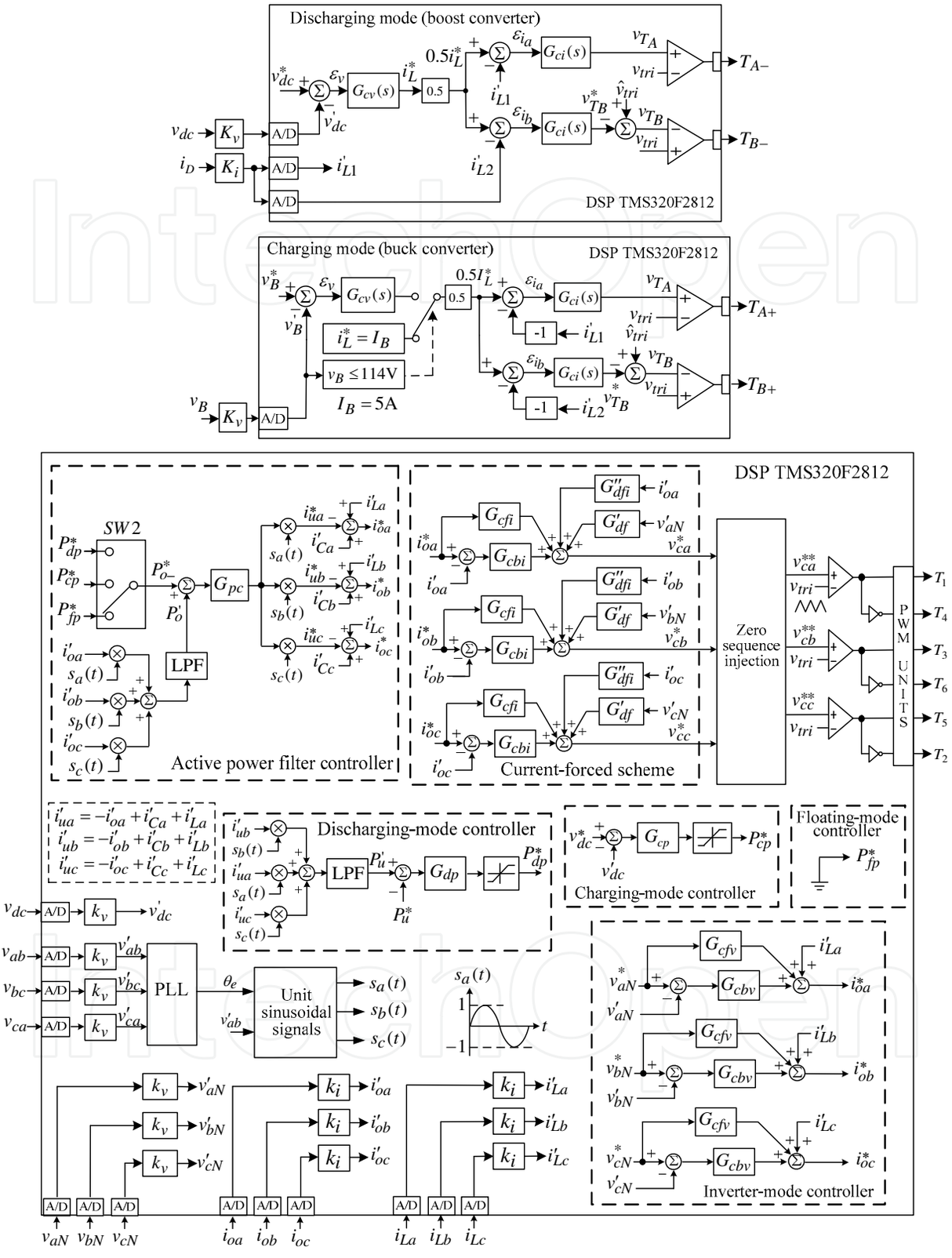
Discharging mode (boost converter)
DSP TMS320F2812
Charging mode (buck converter)
DSP TMS320F2812
DSP TMS320F2812
SW 2
LPF
Active power filter controller
Current-forced scheme
Zero sequence injection
PWM UNITS
Discharging-mode controller
Charging-mode controller
Floating-mode controller
PLL
Unit sinusoidal signals
Inverter-mode controller

(a)

http://dx.doi.org/10.5772/61248

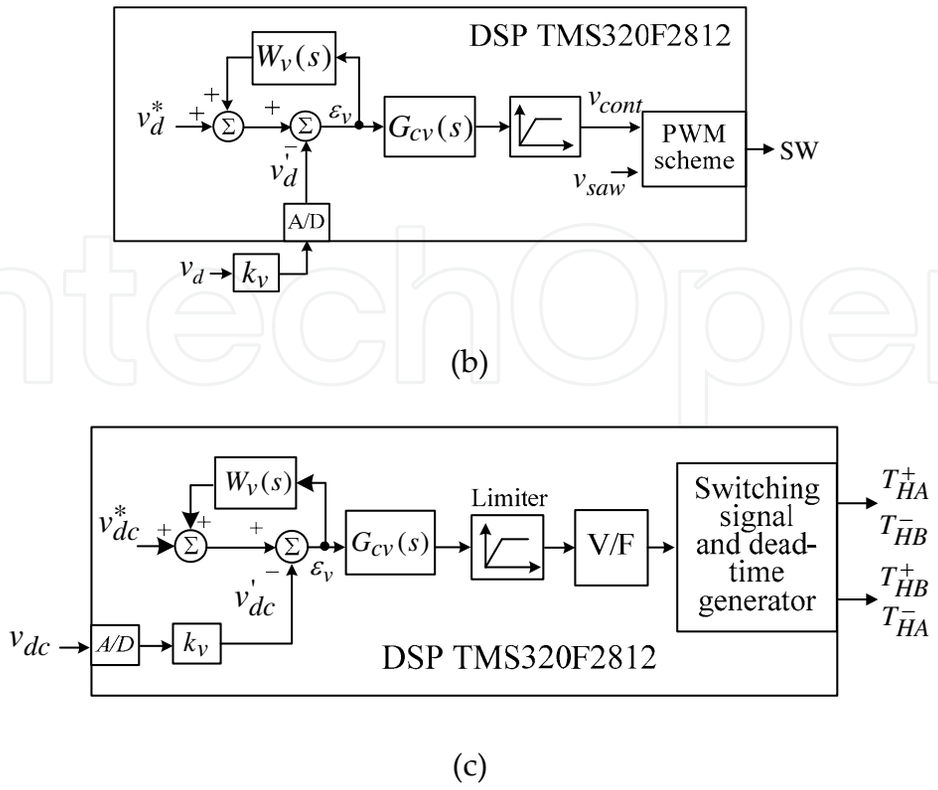


**Figure 12.** Control schemes of the developed grid-connected BESS: (a) BESS in charging mode from grid; (b) 3P1SW SMR in plug-in energy harvesting system; (c) LLC resonant DC/DC converter in plug-in energy harvesting system.

**b.** BESS battery charging from harvested three-phase AC source (E2B)

The harvested three-phase auxiliary AC sources are inputted to the system via the three-phase bridgeless DCM SMR. Through the LLC resonant DC/DC converter, the well-regulated BESS 400 V DC bus voltage is established. And the battery bank is charged from the DC bus via the BESS interleaved DC/DC interface converter in buck mode. The measured ($v_{dc}$, $v_d$, $v_{an}$, $i_{an}$) and ($v_B$, $i_L$ , $i_{L\ 1}$, $i_{L\ 2}$) are shown in Figs. 14(a) and 14(b). Normal and good operation characteristics of all the constituted power stages can be seen from the results. The corresponding measured steady-state characteristics are:

- $P_{in}$ = 721.91, $P_B$ =564.25, $\eta$ = 0.78.
- $i_{an}$ : $\text{THD}_i$ =24.17%, PF=0.963.
- $i_{bn}$ : $\text{THD}_i$ =26.00%, PF=0.955.
- $i_{cn}$ : $\text{THD}_i$ =24.42%, PF=0.962.

**D. Plug-in Energy Harvesting System with Single-phase AC Source and DC Source Inputs**

**a.** Schematic

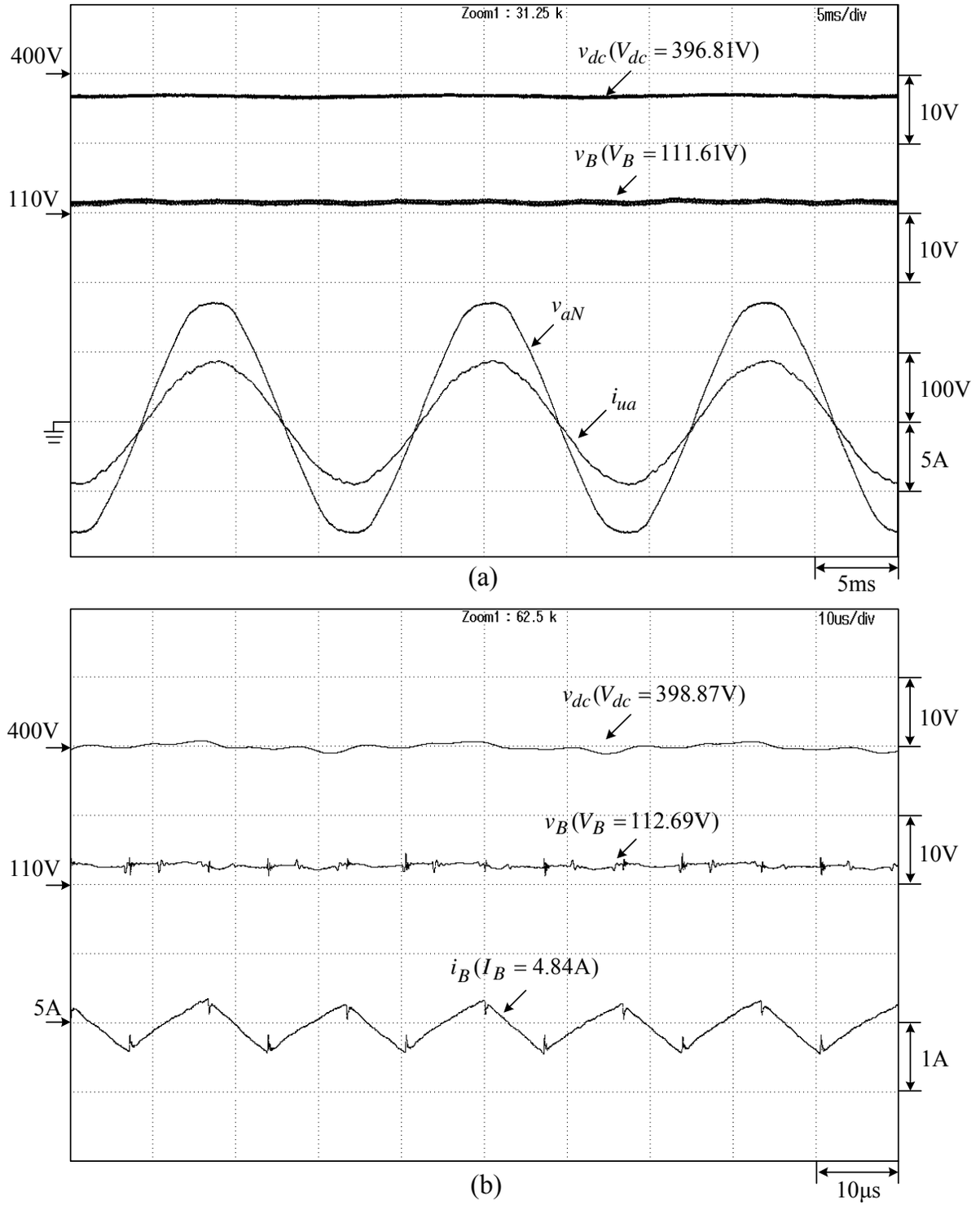


**Figure 13.** Measured results of the established BESS in charging modes at linear resistive and induction motor reactive load: (a) $v_{dc}$, $v_B$ and ($v_{aN}$, $i_{ua}$); (b) $v_{dc}$, $v_B$ and $i_B$.

http://dx.doi.org/10.5772/61248

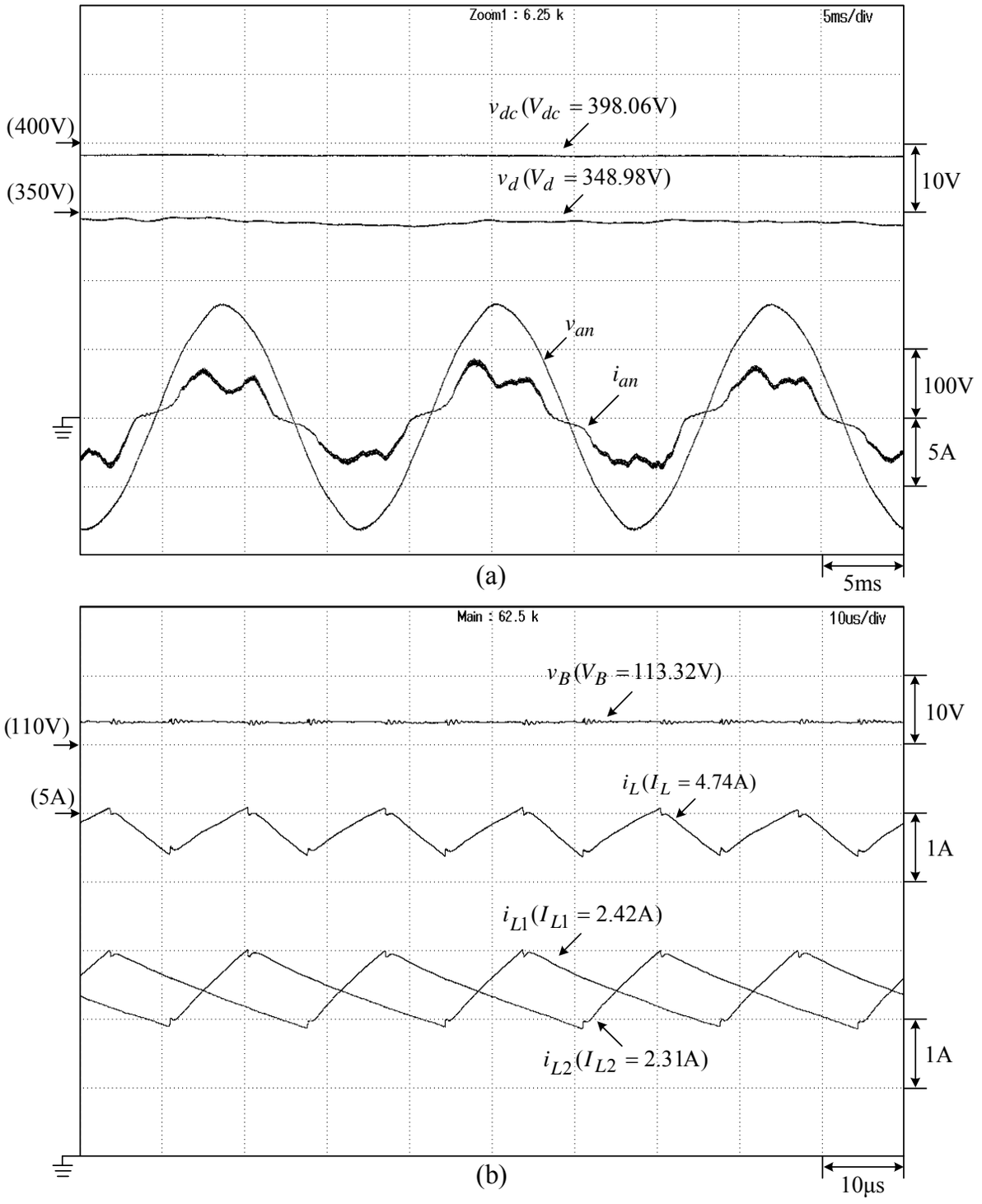


**Figure 14.** Measured results of the developed isolated plug-in energy harvesting system for the BESS battery charging from three-phase AC source with three-phase bridgeless DCM SMR front-end converter: (a) ($v_{dc}$, $v_d$, $v_{an}$, $i_{an}$); (b) ($v_B$, $i_L$ , $i_{L\ 1}$, $i_{L\ 2}$).

The single-phase AC source and DC source can also be inputted to the BESS via the developed plug-in three-phase DCM SMR. The power circuits and control schemes of these two cases are shown in Fig. 15(a) and Fig. 15(b). The single-phase bridgeless boost SMR formed in Fig. 15(a) is operated using a standard SMR control scheme in CCM. Only two extra energy storage inductors ($L_{b1}$, $L_{b2}$) are externally added, and the other constituted circuit components are the embedded ones in the original three-phase SMR. The working switches are $s_1$ and $s_2$ being operated simultaneously.

Some system parameters are set as: (i) PWM switching frequency: $f_s$=37.5kHz ; (ii) DC output voltage $V_d$=350V ; (iii) $v_{ac} \triangleq \sqrt{2V_{ac}}\sin\omega t$, $V_{ac}$=220V ± 10% ; (iv) The inductor current ripple is treated at $\omega t = 0.5\pi$, at which the current ripple is maximum; (v) Total energy storage inductance $L = L_{b1} + L_{b2} + L_{c1} + L_{c2}$. The measured inductances of the two wound inductors $L_{b1}$ and $L_{b2}$ using the HIOKI 3532-50 LCR meter are $L_{b1}$ = (3.55mH, ESR= 183.4mΩ at 60Hz, and 827.0μH, ESR = 124.6Ω at 37.5kHz) and $L_{b2}$ = (3.44mH, ESR= 206.1m Ω at 60Hz, and 794.8μH, ESR =120.7 Ω at 37.5kHz).

**b.** Control schemes

**1.** Current control scheme

- Feedback controller: $G_{ci}(s) = K_{Pi} + \frac{K_{Ii}}{s} = 4.2 + \frac{3150}{s}$
- Robust current error controller (RCEC):

$W_i(s) = \frac{W_i}{1+\tau_i s}$, $W_i$=0.1, $\tau_i = 2.652\times10^{-4}$ (cut-off frequency $1/2\pi\tau_i$=600Hz)

And the current sensing factor is set as $k_i$=0.05V/A.

**2.** Voltage control scheme: $G_{cv}(s) = K_{Pv} + \frac{K_{Iv}}{s} = 1.5 + \frac{39.37}{s}$

**c.** Measured results

A load resistor $R_d$ is placed at the SMR output of Fig. 2 for making the performance test. At the condition of ($v_{ac}$=200V/60Hz, $v_d$=350V, $R_d$=150Ω), the measured stead-state ($v_{ac}$, $i_{ac}$, $i_{ac}^*$, $i_{ac}^{'}$) of the bridgeless single-phase boost SMR formed using the embedded components of the developed plug-in energy harvesting system are plotted in Fig. 16. The corresponding static characteristics are: ($I_{ac}$=4.09A, $THD_i$=3.35%, $PF$=0.997) and ($P_d$=839.1W, $P_{in}$=867.5W, $\eta$=96.72%) with the efficiency being defined as $\eta \triangleq P_d / P_{in}$. The powers are measured using the power analyzer PM100. Good power quality and high energy conversion efficiency are observed from the results.

By replacing the AC input in Fig. 15(a) with the DC source, the DC source harvesting circuit using the three-phase bridgeless DCM SMR embedded components is formed as shown in Fig. 15(b). Its control scheme is also depicted in Fig. 15(b). The energy storage inductors designed in Fig. 15(a) is also suited in this case.

http://dx.doi.org/10.5772/61248

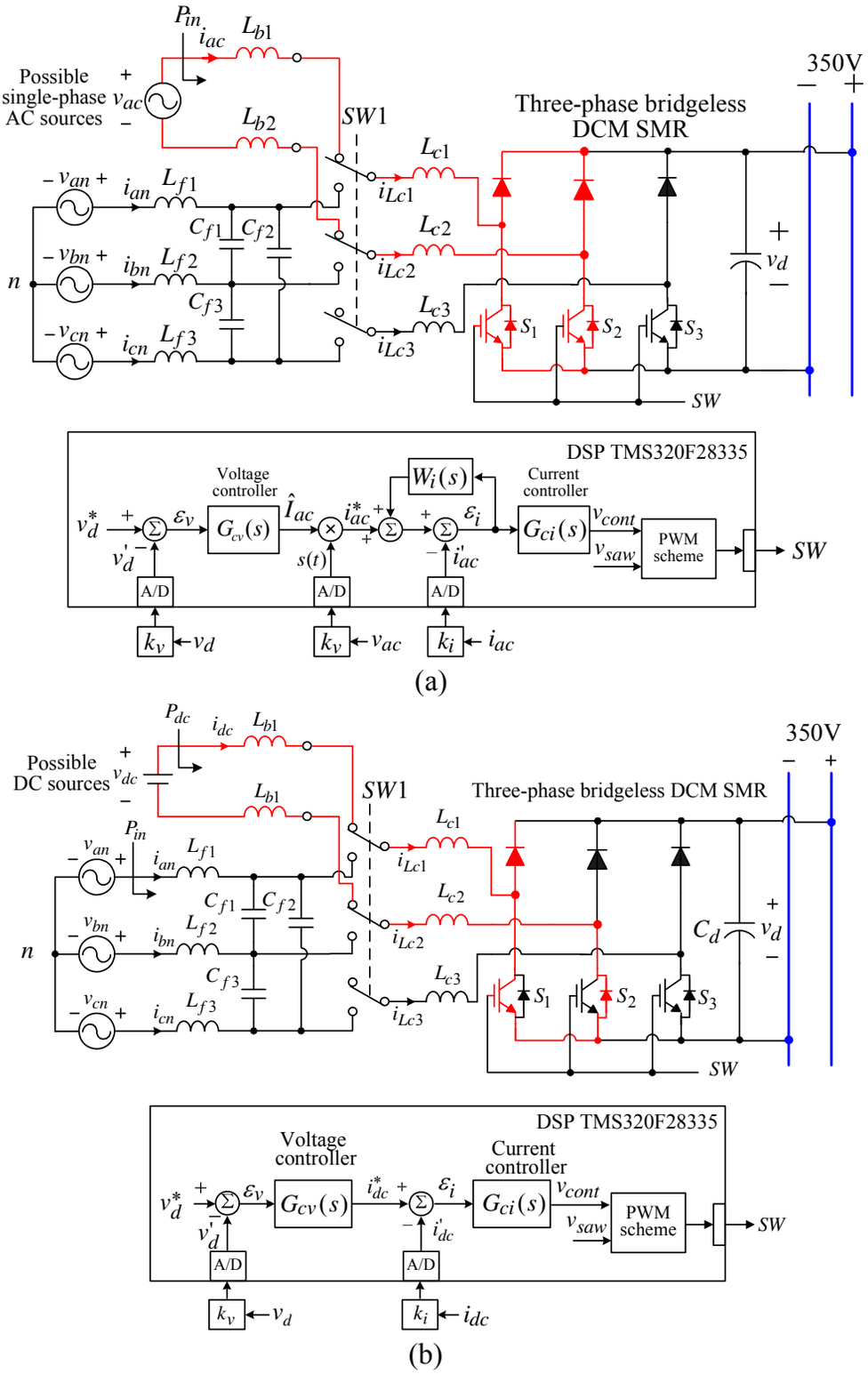


**Figure 15.** The schematics and control schemes of the developed plug-in energy havesting system with single-phase AC source and DC source inputs: (a) single-phase AC source input; (b) DC source input.

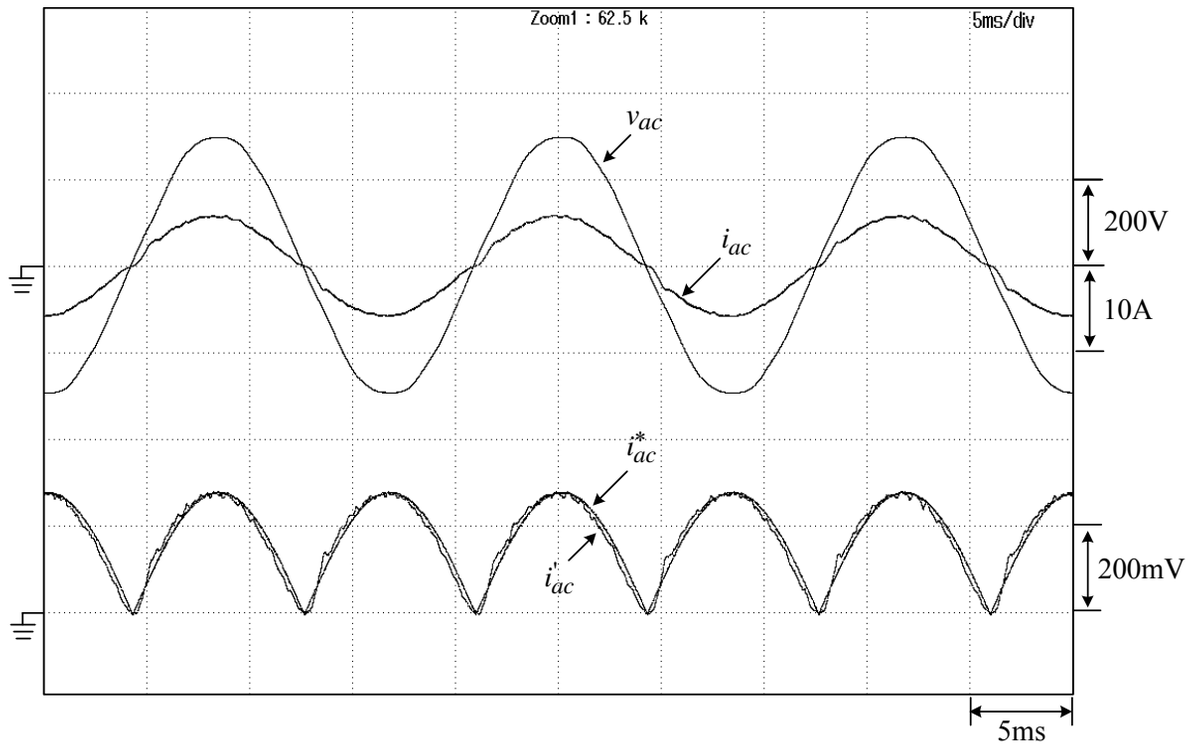


**Figure 16.** Measured ($v_{ac}$, $i_{ac}$, $i^*_{ac}$, $i'_{ac}$) of the bridgeless single-phase boost SMR formed using the embedded components of the developed plug-in energy harvesting system at ($v_d$ =350V, $R_d$ =150Ω).

### 6.3. G2V operation of the IPMSM EV drive with single-phase SMR based battery charger

In the developed EV IPMSM drive shown in Fig. 2, a single-phase and a three-phase boost SMR based chargers can be formed using its embedded circuit components. By placing the changeover switch at the position ②, a two-stage single-phase SMR based battery charger is formed as shown in Fig. 17(a). It consists of an H-bridge boost SMR formed by the two outer inverter IGBT legs and a followed interleaved buck DC/DC converter based charger. Fig. 17(b) shows the proposed control schemes of the two power stages. The batteries are first charged under constant current mode with 0.25 C = 3.5 A. The current of 3.5 A is set by $i^*_{bm}$ in the current limiter at the output of $G_{cv}(s)$. When the battery bank voltage reaches $v_b$=165V, the charging enters constant-voltage floating mode automatically.

**A. System Components**

The constituted system parameters are listed below:

**a.** Interleaved buck DC/DC converter

**i.** Battery bank voltage: $V_b$= 140 ~ 152 V

**ii.** Maximum battery charging voltage: 165 V

http://dx.doi.org/10.5772/61248

**iii.** Maximum battery charging current: $i_b$= 0.25C= 3.5A set by $i_{bm}^*$

**iv.** Switching frequency: $f_s$= 25 kHz

**v.** Energy storage inductors: $L_{b1}$= 4.140mH/25kHz, $L_{b2}$= 4.029mH/25kHz

**vi.** IGBT: STGW35NC60WD by STMicroelectronics Company

**b.** Single-phase SMR

**i.** DC-link voltage: $V_{dc}$= 400V

**ii.** AC input voltage: $V_{AB}$= 220V ± 10% / 60Hz

**iii.** Input energy storage inductors: $L_1$= $L_3$= 0.88mH

**iv.** Output filter capacitor: $C_{dc}$=2200μF / 450V

**v.** Switching frequency: $f_s$= 30kHz

**B. Control Schemes**

**a.** Interleaved buck DC/DC converter

The current and voltage feedback controllers are set as:

$$G_{ci}(s) = K_{Pi} + \frac{K_{Ii}}{s} = 1.2 + \frac{30}{s}, K_i(s) = \frac{K_i}{1+\tau_i s} = \frac{0.1}{1+1.59\times10^{-4}s}$$

$$G_{cv}(s) = K_{Pv} + \frac{K_{Iv}}{s} = 1.5 + \frac{37.5}{s}, K_v(s) = \frac{K_v}{1+\tau_v s} = \frac{0.002}{1+2.65\times10^{-4}s}$$

**b.** Single-phase SMR

The current and voltage feedback controllers are set as:

$$G_{ci}(s) = K_{Pi} + \frac{K_{Ii}}{s} = 0.9 + \frac{2700}{s}, K_i(s) = \frac{K_i}{1+\tau_i s} = \frac{0.125}{1+1.59\times10^{-5}s}$$

$$G_{cv}(s) = K_{Pv} + \frac{K_{Iv}}{s} = 0.1 + \frac{2.5}{s}, K_v(s) = \frac{K_v}{1+\tau_v s} = \frac{0.002}{1+2.65\times10^{-4}s}$$

**C. Experimental Results**

In the single-phase H-bridge boost SMR based charging system shown in Fig. 17(a), the AC input 220 V/60 Hz and the DC-link voltage command $V_{dc}^*$= 400 V are set in G2V operation. By setting the constant current charging with $i_b^*$ to be $i_{bm}^*$=0.25C=3.5A, the measured ($v_{AB}$, $i_{uA}$) and

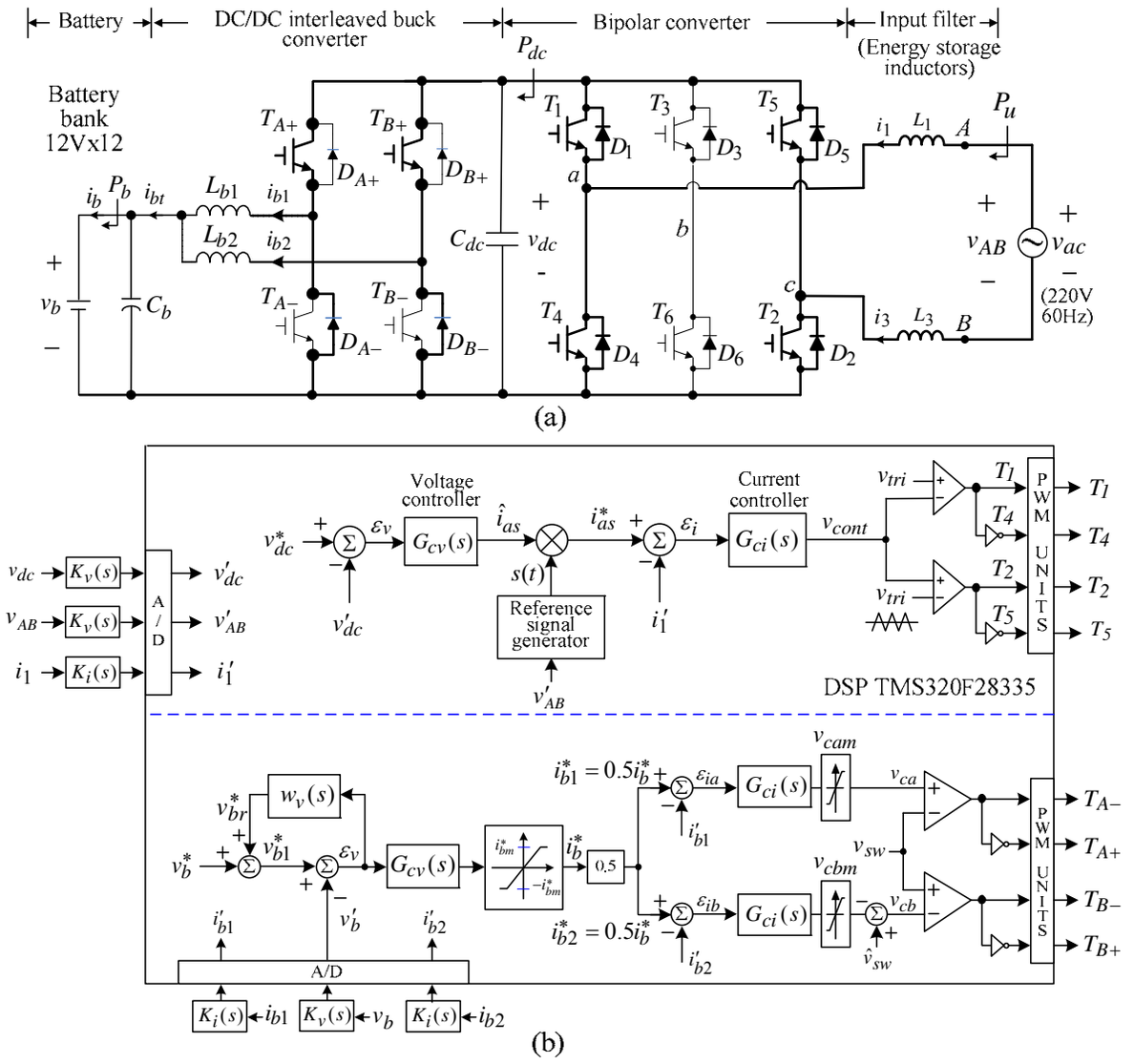


**Figure 17.** System configuration and control scheme of the established single-phase H-bridge boost SMR based battery charger: (a) schematic; (b) control scheme.

($v_b$, $i_b$) of the developed charging system are shown in Figs. 18(a) and 18(b). Satisfactory SMR operation can be observed from the results.

### 6.4. G2V operation of the IPMSM EV drive with three-phase SMR based battery charger

#### A. System Components of Three-phase SMR

**i.** DC-link voltage: $V_{dc}$ = 400 V

**ii.** AC input voltage: $V_{AB}$ = 220V ± 10% / 60Hz

**iii.** Input energy storage inductors: $L_1 = L_2 = L_3$ = 0.88mH

http://dx.doi.org/10.5772/61248

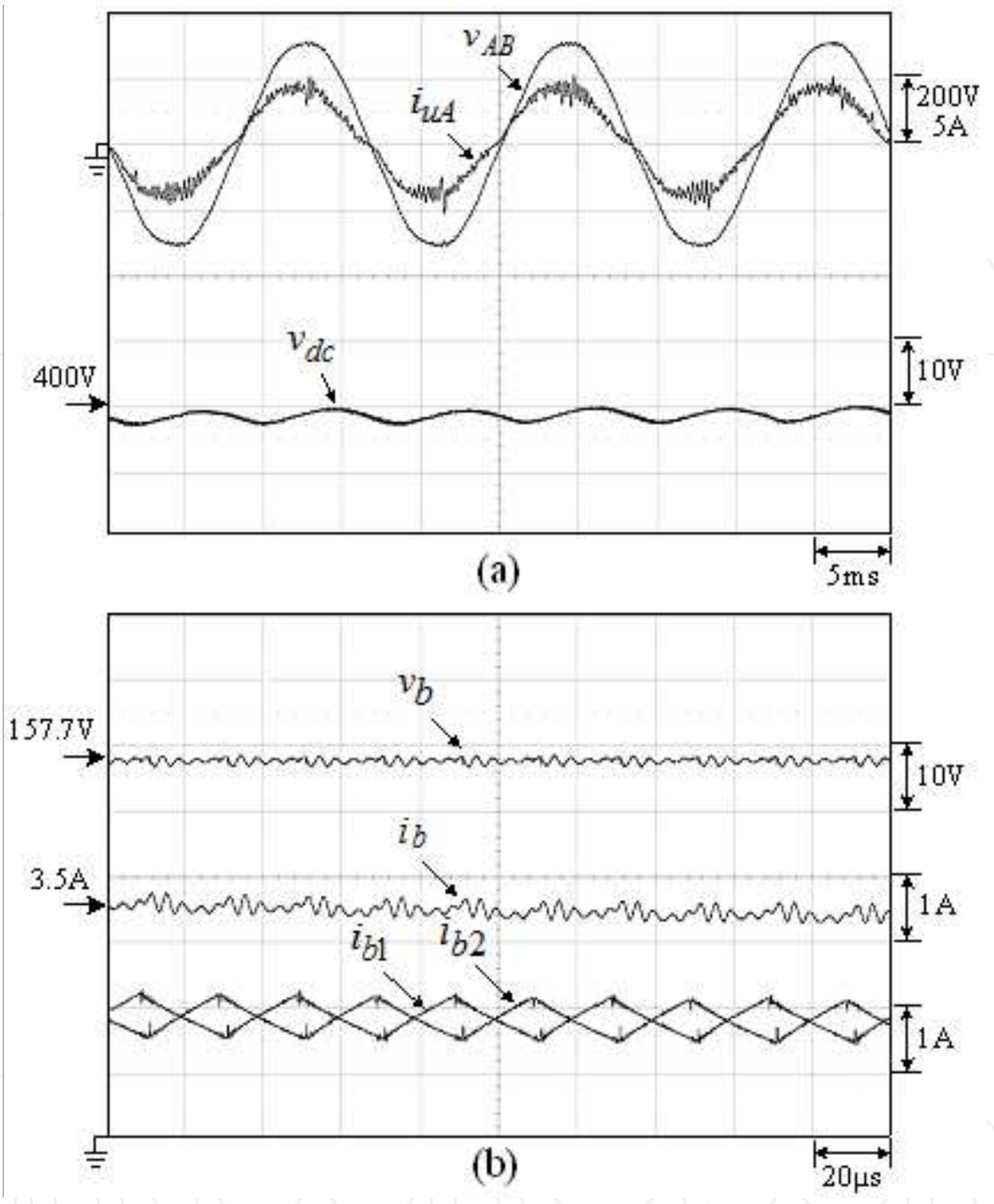


**Figure 18.** Measured results of the established single-phase charging system at ($i_b^*$ = 3.5A, $V_b$ = 157.7V, $V_{dc}^*$ = 400 V, $V_{AB}$ = 220 V/60 Hz): (a) ($v_{dc}$, $v_{AB}$, $i_{uA}$); (b) ($v_b$, $i_b$, $i_{b1}$, $i_{b2}$).

**iv.** Output filter capacitor: $C_{dc}$ = 2200μF / 450V

**v.** Switching frequency: $fs$ = 30kHz

**B. Control Schemes of Three-phase SMR**

The current and voltage feedback controllers are set as:

$$G_{ci}(s) = K_{Pi} + \frac{K_{Ii}}{s} = 2.0 + \frac{50}{s}, K_i(s) = \frac{K_i}{1+\tau_i s} = \frac{0.125}{1+1.59\times10^{-5}s}$$

$$G_{cv}(s) = K_{Pv} + \frac{K_{Iv}}{s} = 0.2 + \frac{10}{s}, K_v(s) = \frac{K_v}{1+\tau_v s} = \frac{0.002}{1+1.59\times10^{-4}s}$$

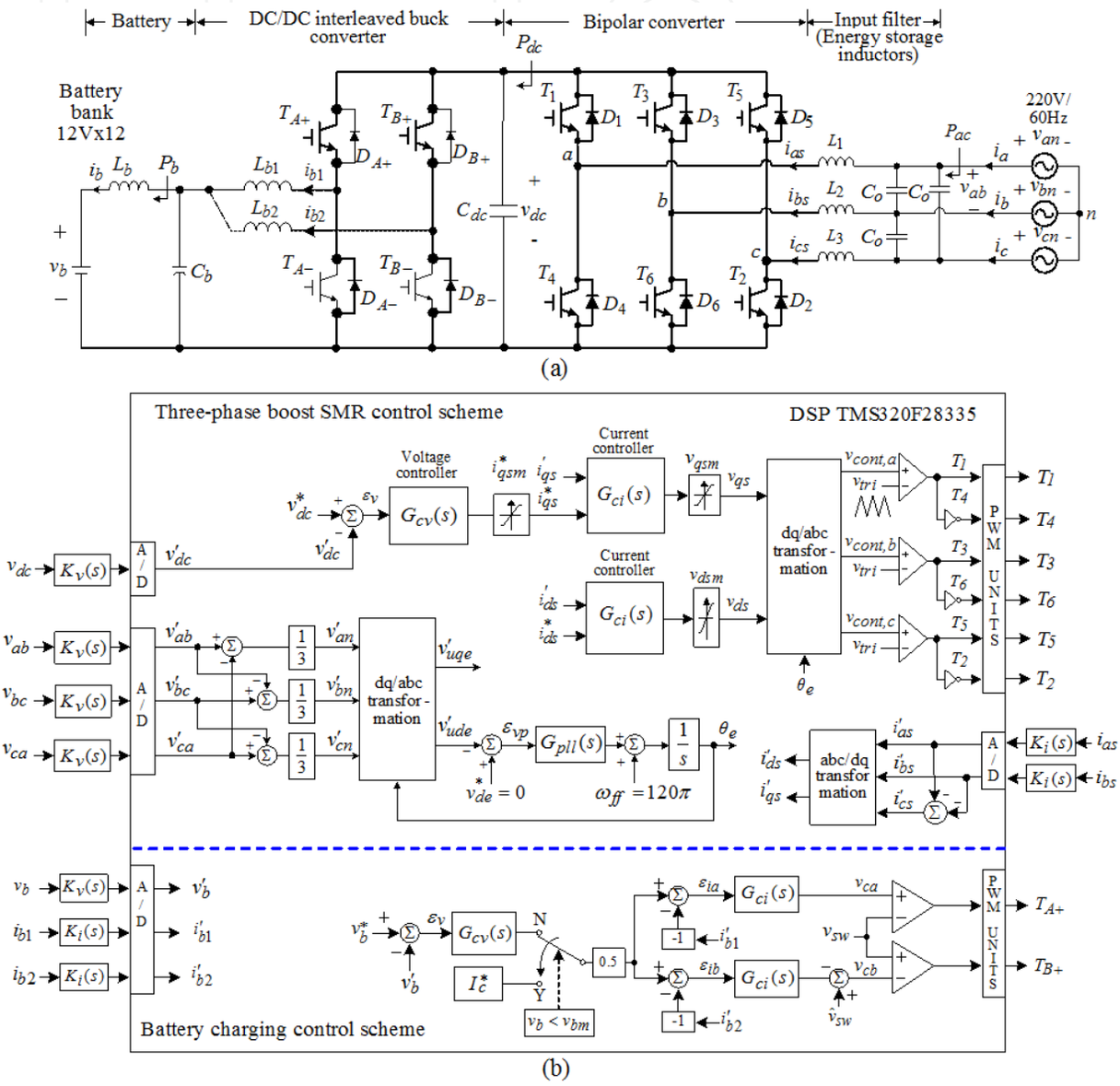


**Figure 19.** Schematic and control scheme of the established three-phase SMR based battery charger: (a) schematic; (b) control scheme.

## C. Experimental Results

Under the conditions of ($V_{ab}$= 220V/60Hz, $V_{dc}^{*}$= 400V, $i_{bm}^{*}$= 0.25C= 3.5A), the measured ($v_{as}$, $i_{as}$) and ($v_b$, $i_b$) of the developed three-phase charging system are shown in Figs. 20(a) and 20(b).

http://dx.doi.org/10.5772/61248

Similarly, good operation performance of the established three-phase SMR based charger is also seen from the results.

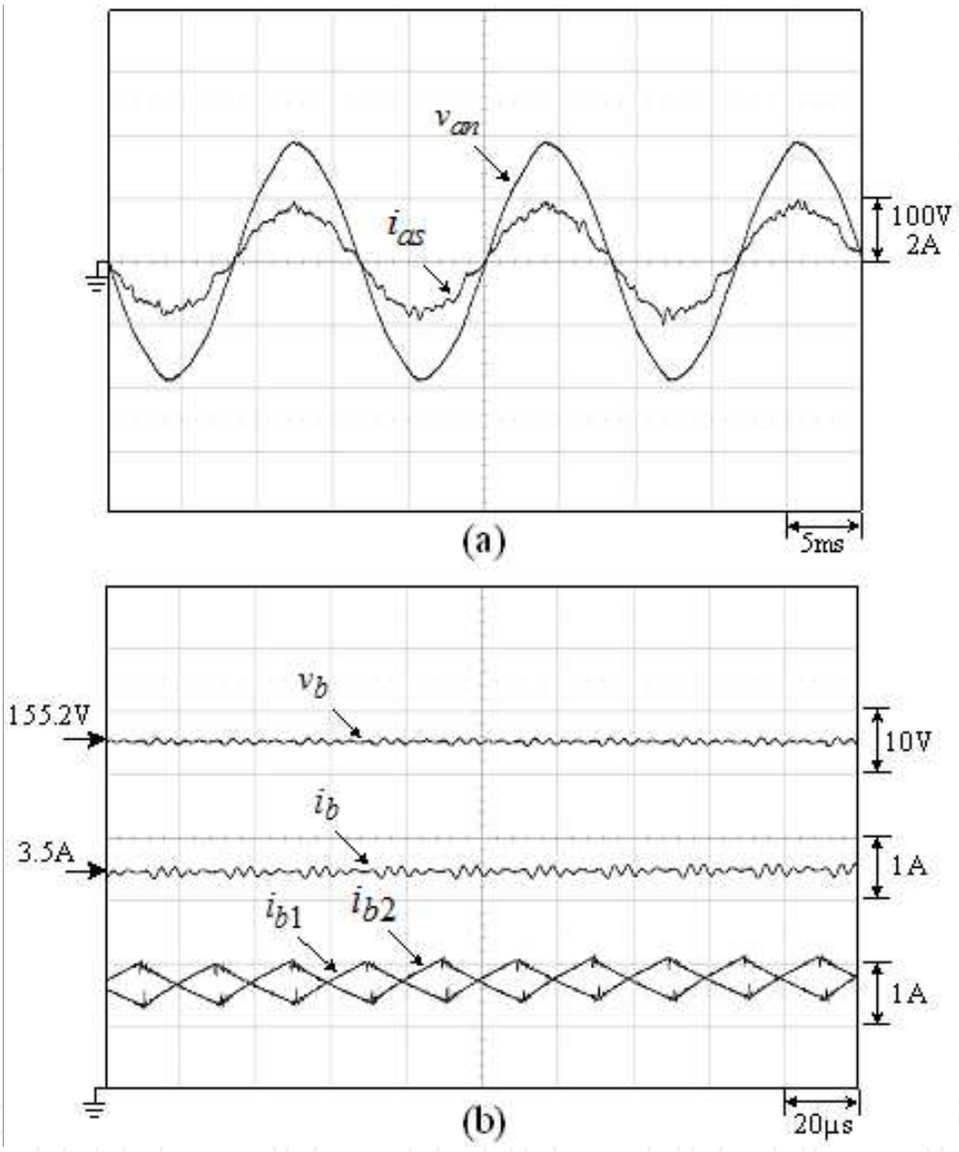


**Figure 20.** Measured ($v_{an}$, $i_{as}$) and ($v_b$, $i_b$) of the established three-phase SMR based battery charger at ($i^*_{bm}$=0.25C= 3.5A, $V_{ab}$= 220V/60Hz, $V_{dc}$= 400V, $V_b$=155.2V): (a) ($v_{an}$, $i_{as}$); (b) ($v_b$, $i_b$, $i_{b1}$, $i_{b2}$).

## 7. Conclusions

Switch-mode rectifier can provide adjustable and well-regulated DC voltage with good AC line drawn power quality. Hence, it has been widely applied in many power electronic equipments to yield improved operation characteristics. However, the schematic and control scheme should be properly selected, designed, and implemented in accordance with the

specific application. During the past decades, the development and employment of micro-grids and EVs have received much attention worldwide for reducing fossil energy comsumption. This article has presented the applications of switch-mode rectifiers on micro-grids incorporating with EV and BESS. After introducing the basics and some key issues of SMRs, the configuration of the studied system is introduced. Then, the applications and performance evalutions of SMRs in micro-grid, BESS, and EV are presented.

Some conclusions and comments for the practical issues of SMRs in the related plants covered in this article are summarized as follows:

1. DC Micro-grid: (i) The 3P3SW Vienna SMR is adopted as the followed converter of wind PMSG. It possesses the advantages of having good compromised characteristics in de-rate, switch number, single-quadrant operation, current PWM control flexibility, and commutation shifting ability. (ii) Load inverter: the bidirectional 1P3W inverter is adopted for providing the 110 V/220 V AC sources for powering the home appliances. It can successfully perform the M2G and G2M operations. In G2M operation, the single-phase SMR is formed to allow the utility supply power to the micro-grid for energy support or for making the battery supplementary charging. The EV can also perform G2V/V2G operations via the micro-grid interface converters.
2. EV PMSM Drive: The developed battery/SC powered EV IPMSM drive possesses G2V/V2H/V2G operation capabilities. In G2V operation, a single-phase boost SMR and a three-phase boost SMR can be formed using the embedded components to charge the battery bank through the bidirectional interleaved buck DC/DC converter with satisfactory line drawn power quality from the mains. The interconnected operations of the EV to the micro-grid and the BESS can also be conducted.
3. BESS: (i) Grid-connected operation: the three-phase six-switch bidirectional inverter can be arranged to operate in G2B charging mode. The utility grid supplies the load real power and also charges the battery bank with good line drawn power quality. The latter task is achieved by arranging the inverter to be operated as a three-phase 4-quadrant SMR with proper control. The BESS can compensate all load reactive and harmonic powers. (ii) Plug-in energy harvesting system: Various AC sources and DC sources can be connected to the BESS via the three-phase bridgeless discontinuous current mode (DCM) SMR through proper schematic and control arrangements. This type of SMR is chosen owing to the single-quadrant operation requirement. In addition, the interconnected operations of the BESS to the micro-grid and EV are also applicable.

## Author details

K. W. Hu and C. M. Liaw*

*Address all correspondence to: cmliaw@ee.nthu.edu.tw

National Tsing Hua University, Taiwan

http://dx.doi.org/10.5772/61248

## References

[1] Ito, Y.; Yang, Z. & Akagi, H. DC microgrid based distribution power generation system. *Proceedings of IEEE International Power Electronics and Motion Control Conference,* pp. 1740-1745, ISBN 7-5605-1869-9.

[2] Hatziargyriou, N.; Asano, H.; Iravani, R. & Marnay, C. Microgrids. *IEEE Power and Energy Magazine,* Vol. 5, No. 4, July-Aug. 2007, pp. 78-94, ISSN 1540-7977.

[3] Boroyevich, D.; Cvetkovic, I.; Dong, D. & Burgos, R. Future electronic power distribution systems a contemplative view. *Proceedings of IEEE Transportation Optimization of Electrical and Electronic Equipment Conference,* pp. 1369-1380, ISBN 978-1-4244-7019-8.

[4] Valderrama-Blavi, H.; Bosque, J.M.; Guinjoan, F. & Marroyo, L. Power adaptor device for domestic DC microgrids based on commercial MPPT inverters. *IEEE Transactions on Industrial Electronics,* Vol. 60, No. 3, March 2013, pp. 1191-1203, ISSN 0278-0046.

[5] Guerrero, J.M.; Vasquez, J.C.; Matas, J.; de Vicuna, L.G. & Castilla, M. Hierarchical control of droop-controlled AC and DC microgrids-A general approach toward standardization. *IEEE Transactions on Industrial Electronics,* Vol. 58, No. 1, January 2011, pp. 158-172, ISSN 0278-0046.

[6] Zeraoulia, M.; Benbouzid, M.E.H. & Diallo, D. Electric motor drive selection issues for HEV propulsion systems : A comparative study. *IEEE Transactions on Vehicular Technology,* Vol. 55, No. 6, November 2006, pp. 1756-1764, ISSN 0018-9545.

[7] Villafafila-Robles, R.; Lloret-Gallego, P.; Heredero-Peris, D.; Sumper, A.; Cairo, I.; Cruz-Zambrano & Vidal, N. Electric vehicles in power systems with distributed generation : Vehicle to microgrid (V2M) project. *Proceedings of IEEE Electrical Power Quality and Utilisation Conference,* pp. 1-6, ISBN 978-1-4673-0379-8.

[8] Hu, K.W. & Liaw, C.M. On a DC microgrid incorporating with electric vehicle as movable energy storage source. *Proceedings of IEEE Internaitonal Conference on Industrial Technology,* March 2015, pp. 2606-2611.

[9] Kramer, B.; Chakraborty, S. & Kroposki, B. A review of plug-in vehicle and vehicle-to-grid capability. *Proceedings of IEEE Indutrial Electronics Conference,* pp. 2278-2283, ISBN 978-1-4244-1767-4.

[10] Madawala, U.K. & Thrimawithana, D.J. Bidirectional inductive power interface for electric vehicle in V2G systems. *IEEE Transactions on Industrial Electronics,* Vol. 58, No. 10, October 2011, pp. 459-473, ISSN 0278-0046.

[11] Verma, A.K.; Singh, B. & Shahani, D.T. Grid to vehicle and vehicle to grid energy transfer using single-phase bidirectional AC-DC converter and bidirectional DC-DC

converter. *Proceedings of IEEE Energy, Automation, and Signal Conference,* pp. 1-5, ISBN 978-1-4673-0137-4.

[12] Kramer, W.; Chakraborty, S.; Kroposki, B.; Hoke, A.; Martin, G. & Markel, T. Grid interconnection and performance testing procedure for vehicle-to-grid (V2G) power electronics. *Technical Report NREL/CP-5500-545005*.

[13] Dehaghani, E.S. & Williamson, S.S. On the inefficiency of vehicle-to-grid (V2G) power flow: Potential barriers and possible research directions. *Proceedings of IEEE Transportation Electrification Conference and Exposition,* pp. 1-5, ISBN 978-1-4673-1407-7.

[14] Ota, Y.; Taniguchi, H.; Nakajima, T.; Liyanage, K.M.; Baba, J. & Yokoyama, A. autonomous distributed V2G (vehicle-to-grid) satisfying scheduled charging. *IEEE Transactions on Smart Grid,* Vol. b3, No. b1, March 2012, pp. 559-564, ISSN 1949-3053.

[15] Yimin, G. & Ehsani, M. Design and control methodology of plug-in hybrid electric vehicles. *IEEE Transactions on Industrial Electronics,* Vol. 57, No. 2, February 2010, pp. 633-640, ISSN 0278-0046.

[16] Yeh, T.H.; Cheng, W.F.; Hu, K.W. & Liaw, C.M. An EV IPMSM drive with supercapacitor energy storage and PV energy harvesting. *R.O.C. 35th Symposium on Electrical Power Engineering*.

[17] Cao, J. & Emadi, A. batteries needs electronics. *IEEE Industrial Electronics Magazine,* Vol. 5, No. 1, March 2011, pp. 27-35, ISSN 1932-4529.

[18] Onar, O.C.; Kobayashi, J. & Khaligh, A. A fully directional universal power electronic interface for EV, HEV, and PHEV applications. *IEEE Transactions on Power Electronics,* Vol. 28, No. 12, December 2013, pp. 5489-5498, ISSN 0885-8993.

[19] Yilmaz, M. & Krein, P.T. Review of battery charger topologies, charging power levels, and infrastructure for plug-in electric and hybrid vehicles. *IEEE Transactions on Power Electronics,* Vol. 28, No. 5, May 2013, pp. 2151-2169, ISSN 0885-8993.

[20] He, J.J.; Hu, K.W. & Liaw, C.M. On a battery/supercapacitor powered SRM drive for EV with integrated on-board charger. *Proceedings of IEEE Internaitonal Conference on Industrial Technology,* March 2015, pp. 2667-2672.

[21] Cao, J. & Emadi, A. A new battery/ultracapacitor hybrid energy storage system for electric, hybrid, and plug-in hybrid electric vehicles. *IEEE Transactions on Power Electronics,* Vol. 27, No. 1, January 2012, pp. 122-132, ISSN 0885-8993.

[22] Blanes, J.M.; Gutierrez, R.; Garrigos, A.; Lizan, J.L. & Cuadrado, J.M. Electric vehicle battery life extension using ultracapacitors and an FPGA controlled interleaved buck-boost converter. *IEEE Transactions on Power Electronics,* Vol. 28, No. 12, December 2013, pp. 5940-5948, ISSN 0885-8993.

[23] Burke, A.F. Batteries and ultracapacitors for electric, hybrid and fuel cell vehicles. *Proceedings of IEEE,* Vol. 95, No. 4, April 2007, pp. 806-820, ISSN 0018-9219.

[24] Vazquez, S.; Lukic, S.M.; Galvan, E.; Franquelo, L.G. & Carrasco, J.M. Energy storage systems for transport and grid applications. *IEEE Transactions on Industrial Electronics,* Vol. 57, No. 12, December 2010, pp. 3881-3895, ISSN 0278-0046.

[25] Hu, K.W. & Liaw, C.M. On a bidirectional adapter with G2B charging and B2X emergency discharging functions. *IEEE Transactions on Industrial Electronics,* Vol. 61, No. 1, January 2014, pp. 243-257, ISSN 0278-0046.

[26] Hu, K.W. & Liaw, C.M. On an auxiliary power unit with emergency AC power output and its robust controls. *IEEE Transactions on Industrial Electronics,* Vol. 60, No. 10, October 2013, pp. 4387-4402, ISSN 0278-0046.

[27] Ustun, T.S.; Ozansoy, C.R. & Zayegh, A. Implementing vehicle-to-grid (V2G) technology with IEC 61850-7-420. *IEEE Transactions on Smart Grid,* Vol. 4, No. 2, June 2013, pp. 1180-1187, ISSN 1949-3053.

[28] Khan, M.A.; Husain, I. & Sozer, Y. Integrated electric motor drive and power electronics for bidirectional power flow between the electric vehicle and DC or AC grid. *IEEE Transactions on Power Electronics,* Vol. 28, No. 12, December 2013, pp. 5774-5783, ISSN 0885-8993.

[29] Yilmaz, M. & Krein, P.T. Review of the impact of vehicle-to-grid technologies on distribution systems and utility interfaces. *IEEE Transactions on Power Electronics,* Vol. 28, No. 12, December 2013, pp. 5673-5689, ISSN 0885-8993.

[30] Liaw, C.M. & Chiang, S.J. Design and implementation of a single-phase three-wire transformerless battery energy storage system. *IEEE Transactions on Industrial Electronics,* Vol. 41, No. 5, October 1994, pp. 540-549, ISSN 0278-0046

[31] Chiang, S.J.; Huang, S.C. & Liaw, C.M. (1995). Three-phase multifunctional battery energy storage system. *IET Electric Power Applications,* Vol. 142, No. 4, July 1995, pp. 275-284, ISSN 1350-2352.

[32] Chiang, S.J.; Liaw, C. M.; Chang, L.C. & Chang, W.Y. Multi-module parallel small battery energy storage system. *IEEE Transactions on Energy Conversion,* Vol. 11, No. 1, March 1996, pp. 146-154, ISSN 0885-8969.

[33] Yoshimi, K.; Osawa, M.; Yamashita, D.; Niimura, T.; Yokoyama, R.; Masuda, T.; Kondou, H. & Hirota, T. Practical storage and utilization of household photovoltaic energy by electric vehicle battery. *Proceedings of IEEE Innovative Smart Grid Technologies,* pp. 1-8, ISBN 978-1-4577-2158-8.

[34] Kawakami, N. & Lijima, Y. Overview of battery energy storage systems for stabilization of renewable energy in Japan. *Proceedings of IEEE Renewable Energy Research and Applications Conference,* pp. 1-5, ISBN 978-1-4673-2328-4.

[35] Peng, S.J.; He, J.J.; Hu, K.W. & Liaw, C.M. Development of a plug-in energy harvesting system for battery energy storage system. *Power Electronics Technology Monthly,* Vol. 12, No. 6, 2014, pp. 49-67.

[36] Caricchi, F.; Crescimbini, F.; Giulii Capponi, F. & Solero, L. Study of bi-directional buck-boost converter topologies for application in electrical vehicle motor drives. *Proceedings of IEEE Applied Power Electronics Conference and Exposition,* pp. 287-293, ISBN 0-7803-4340-9.

[37] Hegazy, O.; Barrero, R.; Van Mierlo, J.; Lataire, P.; Omar, N. & Coosemans, T. An advanced power electronics interface for electric vehicles applications. *IEEE Transactions on Power Electronics,* Vol. 28, No. 12, December 2013, pp. 5508-5521, ISSN 0885-8993.

[38] Hegazy, O.; Van Mierlo, J. & Lataire, P. Analysis, modeling, and implementation of a multidevice interleaved DC/DC converter for fuel cell hybrid electric vehicles. *IEEE Transactions on Power Electronics,* Vol. 27, No. 11, November 2012, pp. 4445-4458, ISSN 0885-8993.

[39] Garcia, O.; Cobos, J.A.; Prieto, R.; Alou, P. & Uceda, J. Single-phase power factor correction: A Survey. *IEEE Transactions on Power Electronics,* Vol. 18, No. 3, May 2003, pp. 749-755, ISSN 0885-8993.

[40] Singh, B.; Singh, B.N.; Chandra, A.; Al-Haddad, K.; Pandey, A. & Kothari, D.P. A Review of single-phase improved power quality AC-DC converter. *IEEE Transactions on Industrial Electronics,* Vol. 50, No. 5, October 2003, pp. 962-981, ISSN 0278-0046.

[41] Singh, B.; Singh, B.N.; Chandra, A.; Al-Haddad, K.; Pandey, A. & Kothari, D.P. A review of three-phase improved power quality AC-DC converter. *IEEE Transactions on Industrial Electronics,* Vol. 51, No. 3, June 2004, pp. 641-660, ISSN 0278-0046.

[42] Kolar, J.W. & Friedli, T. The essence of three-phase PFC rectifier systems- Part I. *IEEE Transactions on Power Electronics,* Vol. 28, No. 1, January 2013, pp. 176-198, ISSN 0885-8993.

[43] Friedli, T.; Hartmann, M. & Kolar, J.W. The essence of three-phase PFC rectifier systems- Part II. *IEEE Transactions on Power Electronics,* Vol. 29, No. 2, February 2014, pp. 543-560, ISSN 0885-8993.

[44] Chai, J.Y.; Chang, Y. C. & Liaw, C. M. On the switched-reluctance motor drive with three-phase single-switch-mode rectifier front-end. *IEEE Transactions on Power Electronics,* Vol. 25, No. 5, May 2010, pp. 1135-1148, ISSN 0885-8993.

[45] Hui, J.; Bakhshai, A. & Jain, P.K. Control and modeling of a wind energy system with a three-phase DCM boost converter and a sensorless maximum point power tracking method. *Proceedings of IEEE Transmission and Distribution Conference and Exposition,* pp. 1-7, ISBN 978-1-4673-1934-8.

[46] Kolar, J.W.; Ertl, H. & Zach, F.C. Design and experimental investigation of a three-phase high power density high efficiency unity power factor PWM (VIENNA) rectifier employing a novel integrated power semiconductor module. *Proceedings of IEEE Applied Power Electronics Conference and Exposition,* pp. 514-523, ISBN 0-7803-3044-7.

[47] Youssef, N.B.H.; Al-Haddad, K. & Kanaan, H.Y. Real-time implementation of a discrete nonlinearity compensating multiloops control technique for a 1.5-kW three-phase/switch/level Vienna converter. *IEEE Transactions on Industrial Electronics,* Vol. 55, No. 3, March 2008, pp. 1225-1234, ISSN 0278-0046.

[48] Hu, K.W. & Liaw, C.M. A position sensorless surface-mounted permanent-magnet synchronous generator and its operation control. *IET Power Electronics,* 2015.

[49] Hao, C. & Aliprantis, D.C. Analysis of squirrel-cage induction generator with Vienna rectifier for wind energy conversion sytem. *IEEE Transactions on Energy Conversion,* Vol. 26, No. 3, September 2011, pp. 967-975, ISSN 0885-8969.

[50] Hao, C.; David, N. & Aliprantis, D.C. Analysis of permanent-magnet synchronous generator with Vienna rectifier for wind energy conversion system. *IEEE Transactions on Sustainable Energy,* Vol. 4, No. 1, January 2013, pp. 154-163, ISSN 1949-3029.

[51] Hu, K.W. & Liaw, C.M. Development of a wind interior permanent-magnet synchronous generator based microgrid and its operation control. *IEEE Transactions on Power Electronics*, Vol. 30, No. 9, September 2015, pp. 4973-4985,ISSN 0885-8993.

[52] Spiazzi, G. & Lee, F.C. Implementation of single-phase boost power-factor-correction circuits in three-phase application. *IE*EE Transactions on Industrial Electronics, Vol. 44, No. 3, June 1997, pp. 365-371, ISSN 0278-0046.

IntechOpen